JOURNAL OF GEOPHYSICAL RESEARCH, VOL. 104, NO. B10, PAGES 23,005–23,022, OCTOBER 10, 1999

Formation of natural gas hydrates in marine sediments 2. Thermodynamic calculations of stability conditions in porous sediments

Pierre Henry

Laboratoire de Géologie de l'Ecole Normale Supérieure (CNRS UMR 8538), Paris

Michel Thomas

Physico-Chimie Appliquée, Institut Francais du Pétrole, Rueil-Malmaison

M. Ben Clennell[1]

Department of Earth Sciences, University of Leeds, Leeds, England

Abstract. A thermodynamic model for hydrate formation is used to compute the solubility of methane in pore water in equilibrium with gaseous methane or methane hydrate or both. Free energy of water in the hydrate phase and of methane in gas bubbles are corrected to account for salt effects and capillary effects. Capillary effects increase the solubility of methane in fluid in equilibrium with either hydrate or gas. Natural sediments have a broad distribution of pore sizes, and the effective pore size for capillary effects is a function of the fraction of the pore space filled by hydrate or gas (phase fraction). The equilibrium conditions for hydrate+water+gas equilibrium thus depend on hydrate and gas phase fraction. Data acquired on Blake Ridge during Ocean Drilling Program Leg 164 show that the base of the hydrate stability there is shifted by -2°C or more with respect to the expected temperature and this shift has been attributed to capillary effects. We show that this explanation would require a very small effective pore radius (20 nm at 30 MPa). Mercury porosimetry indicates that the percolation threshold for Blake Ridge silty claystone is reached at 20-25% phase fraction and corresponds to a 100 nm pore radius. Hydrate and gas phase fraction determined with several independent methods are all lower than this percolation threshold, implying that gas and hydrate fill pores larger than 100 nm. We conclude that additional inhibition factors other than pore size effects must be involved to explain the -2°C bottom-simulating reflector (BSR) shift as an equilibrium phenomenon. Capillary effects may, however, explain other observations such as large variations of the gas hydrate content in the sediment with lithology and porosity and the distribution of hydrate between interstitial hydrate and segregated masses. Capillary effects should also oppose the migration of gas bubbles when gas phase fraction is less than the percolation threshold and make unnecessary the assumption of a hydrate seal impermeable to fluids. Alternatively, we can go some way to explaining the offset position of the BSR by relaxing the assumption that the system is in thermodynamic equilibrium. Nucleation kinetics of hydrate and/or free gas bubbles may be inhibited by confinement of the methane-bearing fluid in small pores. Equilibration may also be limited by possible rates of diffusional transport of gas, water, and salt components or be perturbed by significant flows of fluid or heat through the sediments.

1. Introduction

The attraction of marine scientists to gas hydrate research is no doubt explicable, in part by the remarkable phenomenon of burning snowballs; but it is now well known that clathrates are more than a laboratory curiosity. Indeed, worldwide accumulations of methane hydrates in marine sediments amount to a major reservoir of carbon [e.g., *Kvenvolden*, 1988] that may play a significant role in global climate change, both present [*Paull et al.*, 1991] and past [*Dickens et al.*, 1997a]. The distribution of hydrate with depth in the sediment has been reliably determined at very few sites [*Dickens et al.*, 1997b] and processes by which hydrates accumulate and dissociate in the sediments are not yet well understood.

Occurrence of gas hydrate in the sediment is generally recognized from the presence of a bottom-simulating reflector (BSR) and this reflector is generally assumed to represent the three-phase gas+hydrate+water equilibrium. The temperature at the depth of the BSR generally agrees, within 1° or 2°C, with laboratory data for the methane gas+hydrate+pure water equilibrium for bulk phases and, accordingly, geothermal heat flow on continental margins is often derived from BSR depths

[1]Now at Centro de Pesquisa em Geofisica e Geologia, Universidade Federal da Bahia, Salvador, Bahia, Brasil

Paper number 1999JB900167.
0148-0227/99/1999JB900167$09.00

[e.g., *Hyndman et al.*, 1992]. It is well known that the presence of trace gases such as CO_2, ethane and H_2S [*Hovland et al.*, 1995], and the salt concentration in the pore fluids [*Dickens and Quinby-Hunt*, 1997] affect the stability conditions of the hydrate but the influence of the sediment itself has rarely been considered (but see *Ginsburg and Soloviev* [1998, pp. 189-192]). Laboratory experiments show, however, that formation of hydrate and of gas bubbles in porous material are inhibited by surface (or capillary) effects [*Handa and Stupin*, 1992; *Yousif and Sloan*, 1991]. Capillary effects may significantly affect the stability conditions of gas hydrate in fine-grained sediments [*Clennell, et al.*, 1995] and were invoked to explain the abnormally low temperatures measured at the base of the hydrate stability field on Blake Ridge [*Ruppel*, 1997].

Models for the formation of hydrate in porous sediments that ignore the effect of pore size predict a constant hydrate concentration with depth in the sediment, except at the very base of the hydrate stability field where upward migration of gas bubbles may cause accumulation of hydrate [*Rempel and Buffet*, 1997]. Most geophysical studies based on seismic reflection data do not have enough resolution to invalidate this model, but observations in drill holes (Ocean Drilling Program (ODP) Leg 146 on Cascadia margin and ODP Leg 164 on Blake Ridge) show that the distribution of hydrate with depth is more complex [*Dickens et al.*, 1997b] and displays large variations with depth at the scale of a few meters [*Paull et al.*, 1996]. We propose that these variations are caused mainly by capillary effects and are the expression of subtle changes in sediment lithology. Capillary effects may also control the hydrate growth forms observed in marine sediment [*Clennell et al.*, this issue] and presumably influence the formation and migration of gas bubbles beneath the hydrate zone.

In a companion paper, a conceptual model for hydrate formation is built on an analogy between hydrate in marine sediment and ice in permafrost [*Clennell et al.*, this issue]. For the case of hydrate BSRs, the behavior of the free gas phase also requires attention: capillary effects inhibit growth of gas bubbles and cause supersaturation of the pore fluid. The present work is an attempt to evaluate the conceptual model within an equilibrium thermodynamic framework and to quantify how surface effects on both the hydrate and the gas phases modify the phase diagram and equilibrium conditions of the hydrate-methane-pore water system.

Testing the relevance of our model for natural cases requires precise knowledge of the in situ conditions: pressure, temperature, hydrate content, gas content, sediment lithology, and pore size distribution. At present, the only location for which such a complete data set may be available is the Blake Ridge at the ODP Leg 164 drill sites [*Paull et al.*, 1996]. For this reason, most of our discussion will be centered on the Blake Ridge example. We shall summarize in the next section observations that may be attributed to capillary effects, but the reader should refer to the companion paper [*Clennell et al.*, this issue] for a more complete description.

Our thermodynamic model is an adaptation of existing models for bulk hydrate [*Bishnoi et al.*, 1989; *Holder et al.*, 1988; *Munck et al.*, 1988; *Tohidi et al.*, 1995; *Van der Waals and Platteeuw*, 1959]. When combined with a methane equation of state [*Duan et al.*, 1992], this model may be used to compute the gas-water and hydrate-water equilibria as well as the three-phase equilibrium (which, presumably, corresponds to the conditions at the BSR). Surface effects are treated as corrective terms (computed from pore sizes and interfacial energies) in the free energy of the hydrate and gas phases. We limit our analysis to equilibrium cases and will consider issues related to hydrate/gas nucleation only in the discussion section.

We compare our model predictions for the three-phase equilibrium near 0°C with experimental results on hydrate in synthetic porous materials [*Handa and Stupin*, 1992]. These synthetic porous materials may be considered as having a single pore size because their pore size distribution are so narrow [*Handa et al.*, 1992]. Real sediments have a broader distribution and a nonwetting phase (gas, ice, hydrate) will preferentially occupy the largest pores available, in order to minimize surface energy. This implies that the magnitude of surface effects in sediment will depend on the fraction of the pore space filled by each nonwetting phase. Consequently, the predicted gas-hydrate-pore water equilibrium will depend on the pore fractions filled by both hydrate and gas.

The progressive rise of capillary pressure during invasion of the porous network by a non-wetting fluid is precisely what is measured in mercury porosimetry tests [*Arnould, et al.*, 1980, *Lowell and Shields*, 1984]. For this reason, we used data from mercury injection tests to characterize the pore size distribution in Blake Ridge sediments. It is remarkable that even in these clay rich sediments, a large fraction of the pores have a radius of more than 100 nm. The presence of these relatively large pores limits the influence which mineral surfaces may have on hydrate stability.

2. Observations and Problems

There are two different types of observations that we seek to explain with capillary effects: deviations of observed BSR depths from bulk hydrate-water-gas equilibrium and the heterogeneity of the hydrate distribution within its zone of stability.

Seismic reflection studies (notably using amplitude versus offset and waveform inversion methods) show that the BSR is generally caused by the presence of gas in the sediment immediately beneath it [*Singh et al.*, 1993; *Singh and Minshull*, 1994; *MacKay et al.*, 1994; *Katzman et al.*, 1994; *Andreassen et al.*, 1995]. Only a small gas content is needed for this effect to occur and the fraction of pore space filled by gas bubbles is estimated to less than 5% in most geophysical studies [*Singh and Minshull*, 1994; *Holbrook et al.*, 1996; *Yuan et al.*, 1996]. Consequently, the BSR should generally be interpreted as the top of the free gas zone. At ODP sites where a BSR has been drilled (on the Cascadia margin and on Blake Ridge), geophysical and drilling data indicate that the BSR also coincides with the deepest occurrence of gas hydrate [*Whiticar et al.*, 1995; *Kastner et al.*, 1995; *MacKay et al.*, 1994; *Paull et al.*, 1996; *Ruppel*, 1997; *Dickens et al.*, 1997b] (Figures 1 and 2). The BSR is thus inferred to represent the base of the hydrate stability field and a three-phase equilibrium [*Minshull et al.*, 1994; *Ruppel*, 1997]. However, the base of the hydrate stability field is generally found at a shallower level and at a lower temperature than predicted from bulk phase equilibrium, with seawater as fluid [*Clennell et al.*, this issue]. This shift (10-20 m and 0.3°-0.6°C) is small for the Cascadia site but is 1°-3°C (30-100 m) for the Blake Ridge sites (Figure 1)[*Ruppel*, 1997]. *Ruppel* [1997] investigated possible causes for this upward shift and retained capillary inhibition in the fine-grained sediment as the most likely explanation because

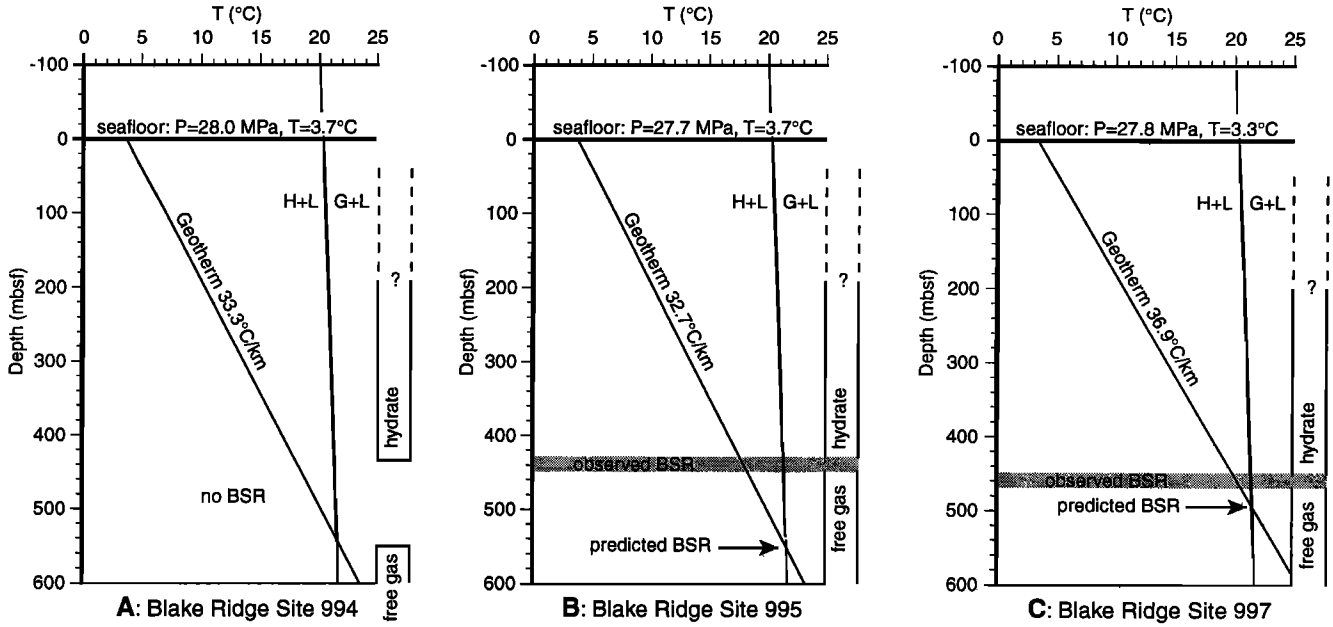

Figure 1. Summary of observations at Blake Ridge ODP site. The depth range of hydrate or free gas are shown [*Dickens et al.*, 1997b; *Holbrook et al.*, 1996; *Paull et al.*, 1996]. (a) At Site 994 there is a gap between the base of the hydrate and the top of the free gas and there is no BSR. (b) At Site 995 and (c) Site 997, the BSR coincides with both the base of the hydrate and the top of the gas. The BSR (bottom-simulating reflector) is thus expected at the intersection between the observed geotherm [*Ruppel*, 1997] and the three-phase-equilibrium curve (H, hydrate; L, Liquid, G; gas). At Site 995 the transition from hydrate to gas is observed more than 100 m above the predicted bulk phase equilibrium. The three-phase equilibrium curve plotted on the graphs is for bulk phase methane gas+seawater+hydrate equilibrium. Capillary effects are not taken into account.

it seemed that no other mechanism could account for the observations. The chemical composition of the pore fluid is fairly typical for sediments undergoing burial under anoxic conditions and excursions in salinity sufficient to shift the phase boundary appreciably have not been detected [*Paull et al.*, 1996]. Other gases (carbon dioxide, ethane and higher hydrocarbons) are present only in minor or trace proportions in core headspace and pressure core sampler (PCS) samples. If present in significant proportions these gases would contribute to increase hydrate stability relative to pure methane hydrate and thus would have an opposite effect as wanted. Finally, transient thermal models of response to climate change also predict a deeper BSR [*Ruppel*, 1997]. The observation, at another location on Blake Ridge, of a faulted BSR structure [*Rowe and Gettrust*, 1993] is another example of BSR irregularities that could be interpreted either as a thermal transient feature or as evidence that hydrate BSRs do not always correspond to a univariant phase boundary.

As shown on Figure 1, the three Blake Ridge sites are not equivalent. The temperature extrapolated at the base of the hydrate zone is 17.2°-18.9°C at Site 994, 17.4°-18.8°C at Site 995, and 19.8°-21.1°C at Site 997 [*Ruppel*, 1997]. Conversely, the distance between the observed BSR depth and the depth predicted from bulk equilibrium (seawater + hydrate +

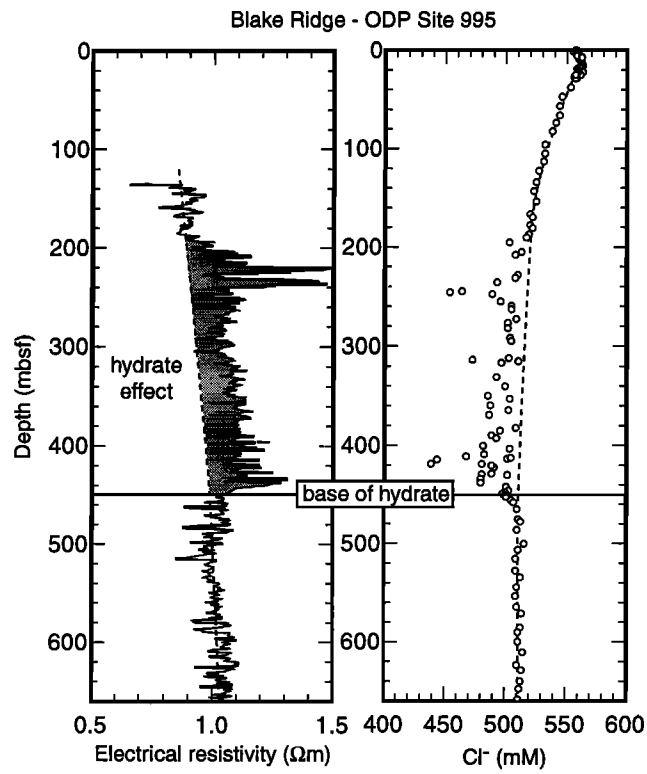

Figure 2. Deep-reading induction resistivity log and pore fluid chlorinity at Blake Ridge Site 995 shows that the distribution of hydrate with depth is highly heterogeneous. The zone where an hydrate effect is observed extends between 200 mbsf (meters below seafloor) and the BSR (base of hydrate). Sharp spikes on the resistivity log at 210-250 mbsf and at 380-450 mbsf correlate with low chlorinity anomalies and correspond to hydrate accumulations. Hydrate fills about 5% of the pore space in average but may fill up to 20-25% of the pore space in these layers.

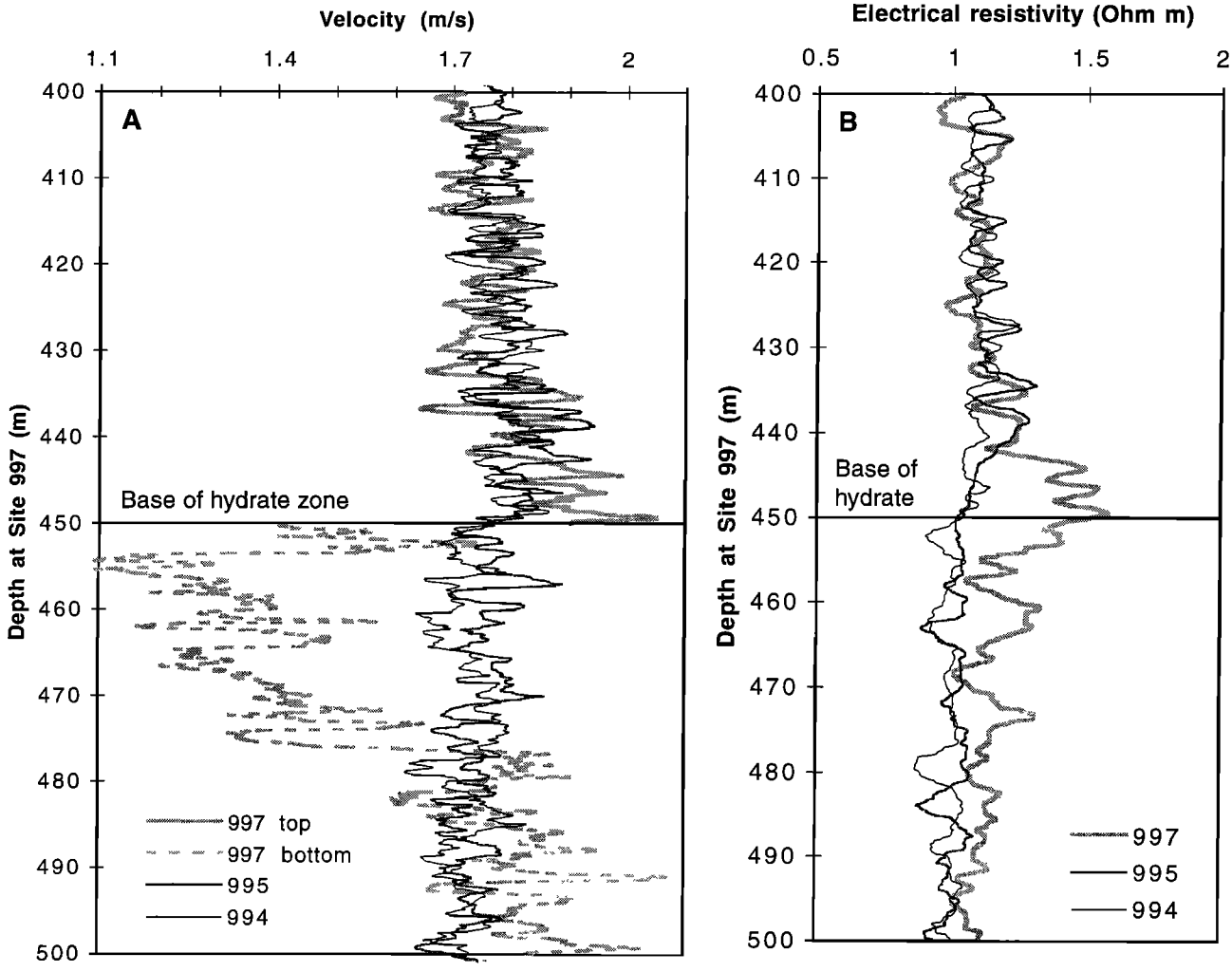

Figure 3. Logging data around the BSR from ODP Leg 164 on Blake Ridge. Depths at Sites 994 and 995 have been adjusted so that the inferred base of the hydrate stability field coincides at all three sites (994, 995, and 997). The base of the hydrate stability field coincides with the BSR at Sites 995 and 997, where a BSR in observed. (a) Acoustic velocity logs. High gas content below the BSR at Site 997 causes large perturbations, and values in this section are not reliable (dashed curve). (b) Deep-reading induction resistivity. Resistivity increases in the hydrate zone is due to pore obstruction by the nonconducting hydrate phase. The resistivity anomaly extends in the gas zone only at site 997.

free gas) is larger (about 100 m) at Site 995 than at Site 997 (20-40 m). Because there is no BSR at Site 994, free gas is presumably absent at the base of the hydrate zone, and this is confirmed by the absence of gas-related anomalies above 550 m below seafloor (mbsf) on the vertical seismic profile (VSP) [*Holbrook et al.*, 1996] and on the velocity and resistivity logs [*Paull et al.*, 1996]. Both chlorinity anomalies and log data nevertheless indicate that the base of hydrate occurrence is sharp and lies between 427 and 440 mbsf. This shows that the deepest occurrence of gas hydrate is not necessarily marked by a reflector. If this limit corresponds to a two-phase equilibrium between hydrate and water with dissolved gas, it may lie well above the depth of the three-phase equilibrium without any need for capillary effects or any other inhibition mechanism. In contrast, Site 997 shows a large gas-related anomaly at the base of the hydrate zone on the VSP as well as on the velocity logs. Resistivity logs (Figure 3) suggest that hydrate phase fraction (the fraction of pore space filled by hydrate S_h) above the BSR and gas phase fraction (the fraction of pore space filled by gas S_g) below the BSR have similar values.

Gas content in a PCS sample taken immediately below the BSR at Site 997 is about 2 mol per dm^3 of pore space, corresponding to a gas phase fraction of 12% [*Dickens et al.*, 1997b]. At Site 995, presence of free gas was inferred from a PCS sample taken 50 m beneath the BSR (490 mbsf) [*Dickens et al.*, 1997b]. The velocity anomaly immediately below the BSR that can be attributed to the presence of gas is small on the VSP [*Holbrook, et al.*, 1996] and resistivity and velocity logs from Site 995 give no further evidence for gas. The similarity of the logs across the base of the hydrate zone at Sites 994 and Site 995 (Figure 3) indicates that S_g is much smaller than S_h at Site 995 and probably not more than 1%. We speculate whether the increase of temperature at the base of the hydrate stability field between Site 995 and Site 997 is related to the increase in gas phase fraction and whether this behavior may be explained by capillary effects.

Estimations by geophysical methods of the average percentage of the pore space filled with hydrates suggest a wide variation (5 to 30%) in different study areas, with some inconsistencies evident where more than one method is used [*Holbrook et al.*, 1996; *Minshull et al.*, 1994; *Yuan et al.*,

1996; *Lee et al.*, 1993]. The spatial distribution of hydrate above the BSR may of course be highly heterogeneous at any given site. At Blake Ridge sites, the zone where the hydrate affects sediment physical properties (detected by downhole logs) and causes significant freshening of the pore fluid when dissociated (measured on core samples; this method is believed to be the most robust and quantitative) does not extend all the way to the seafloor (Figure 2). Within the zone where these hydrate effects are observed, a high dispersion of the chlorinity data and sharp spikes in the resistivity logs at 200-250 and 380-450 mbsf (Figure 2) show that hydrate distribution is highly heterogeneous at the 1-10 m scale, with a hydrate phase fraction varying from nearly 0% to 10 or 20% [*Paull et al.*, 1996]. These variations were also observed with temperature measurements made in the cores after recovery [*Paull et al.*, 1996]. This small-scale heterogeneity is surprising because the lithological profile seems very monotonous throughout the Blake Ridge section, consisting mainly of silty clays and calcareous oozes (see *Clennell et al.* [this issue, Figure 3]). The hydrate content has, however, a weak but positive correlation with sediment grain size [*Ginsburg, et al.*, 1999] and hydrates also tend to be more abundant in a lithological unit rich in siliceous microfossils that provide empty cavities of radius 10-20 μm [*Kraemer, et al.*, 1999]. This suggests that the pore size distribution is an important factor controlling the hydrate content in the sediment.

3. Theoretical Model

One of the main incentives for the development of thermodynamic models for hydrate formation has been their industrial application: gas hydrates can form in pipelines and cause clogging. Models relevant to this problem must treat cases with complex mixtures of gases and must include chemical inhibitors. In contrast, natural gas present in the hydrate stability field is often biogenic gas composed mainly of methane containing only traces of higher hydrocarbons [*Ginsburg and Soloviev*, 1997; *Kvenvolden*, 1988]. This important simplification is, however, balanced by additional complications. Laboratory experiments used for model calibration and industrial application cases always include a free gas phase but not always a liquid water phase, whereas natural gas hydrates in the deep ocean generally occur under the opposite condition: a liquid water phase is always present but not always free gas. Within the hydrate stability field, gas should not be present as a separate phase, and a two-phase divariant equilibrium between hydrate and water with dissolved methane should be assumed [*Ginsburg and Soloviev*, 1997; *Handa*, 1990; *Hyndman and Davis*, 1992; *Miller*, 1974; *Rempel and Buffet*, 1997; *Tohidi, et al.*, 1995; *Zatsepina and Buffett*, 1997], rather than a three-phase (hydrate-water-gas) univariant equilibrium.

There are no systematic measurements of methane solubility in the hydrate stability field, but the corresponding equilibrium can be computed from thermodynamic models [*Miller*, 1985; *Handa*, 1990; *Tohidi, et al.*, 1995; *Zatsepina and Buffett*, 1997, 1998]. For this purpose, we combined a thermodynamic model for hydrate formation [*Munck et al.*, 1988] with a model for methane solubility based on a virial equation of state (EOS) [*Duan et al.*, 1992]. Dissolved salts act as inhibitors and must then be taken into account [*Dickens and Quinby-Hunt*, 1997; *Tohidi, et al.*, 1995]. We have simplified the approach for seawater, using salinity rather than concentration of individual ions (see Appendix). The question of the influence of the sediment is still a matter of debate [*Clennell, et al.*, this issue]. The method chosen here to estimate the capillary effects is to examine independently the displacement of the hydrate-water and water-gas equilibria in a sediment with small pores. The three phase equilibrium is then obtained as the intersection of the two-phase equilibrium curves computed for a given methane fugacity.

3.1. Hydrate-Water Curve

A first approximation of the solubility of methane in a solution in equilibrium with a methane hydrate but in the absence of a free gas phase may be obtained assuming a constant number n of water molecules per methane molecule in the hydrate and constant partial molar volumes of water and methane in both liquid and hydrate phases [*Miller*, 1974]. However, these molar volumes and the probability that a cage is occupied in the hydrate structure vary with temperature as well as with the hydrostatic pressure [*Sloan*, 1990]. A solution of this problem with a more complete thermodynamic treatment is given by *Handa* [1990]. In his model, variations of n are computed with the assumption that the ratio of occupancies (η_1/η_2) for the small and large cages of structure I hydrate is constant. The comparison of the curves obtained by *Handa* [1990] with curves computed with the same equations and volumetric parameters but assuming instead a constant ratio n=6 shows that the variation of hydrate composition with hydrostatic pressure is not a critical parameter (see Appendix). The equation giving the variation of methane solubility x_{CH_4} (in mole fraction) as a function of hydrostatic pressure P can be simplified as

$$\frac{\partial \ln x_{CH_4}}{\partial P} = \frac{1}{RT}\left(n\left(V_\beta - V_L\right) - V^l_{CH_4}\right) = \frac{\Delta V}{RT} \qquad (1)$$

without changing the results significantly. V_β is the molar volume of water in the hydrate lattice, V_L is the partial molar volume of water in the liquid phase and $V^l_{CH_4}$ is the partial molar volume of methane in the liquid phase. ΔV represents the volume change when hydrate is formed out of dissolved methane. ΔV is negative, which means that the methane with its hydration shell occupies less volume in the hydrate than in water, even though a fraction of the cages are empty in the hydrate phase.

Handa [1990] computed equilibrium solubility at 0°C and 5°C and, in part because of the assumption that (η_1/η_2) is constant, his method is difficult to extrapolate to higher temperatures. Thermodynamic models of hydrate stability all predict an increase of the cage occupancies along the hydrate+water+free gas equilibrium curve when temperature and pressure increases, such that practically all the cages should be filled at 25°C and 50 MPa ($n \cong 5.75$). These models, originating from the work of *Van der Waals and Platteeuw* [1959] are now standard [*Holder et al.*, 1988, *Munck et al.*, 1988, *Bishnoi, et al.*, 1989, *Tohidi, et al.*, 1995] and some have already been adapted to compute hydrate-aqueous solution equilibria [*Zatsepina and Buffett*, 1997, 1998]. In this study, we developed a similar approach: details of the computations performed are given in the Appendix and results are compared with existing models. Because the methane saturation curves only weakly depend on P (Figure 4), methane solubility in the presence of hydrate can be computed as a function of temperature only.

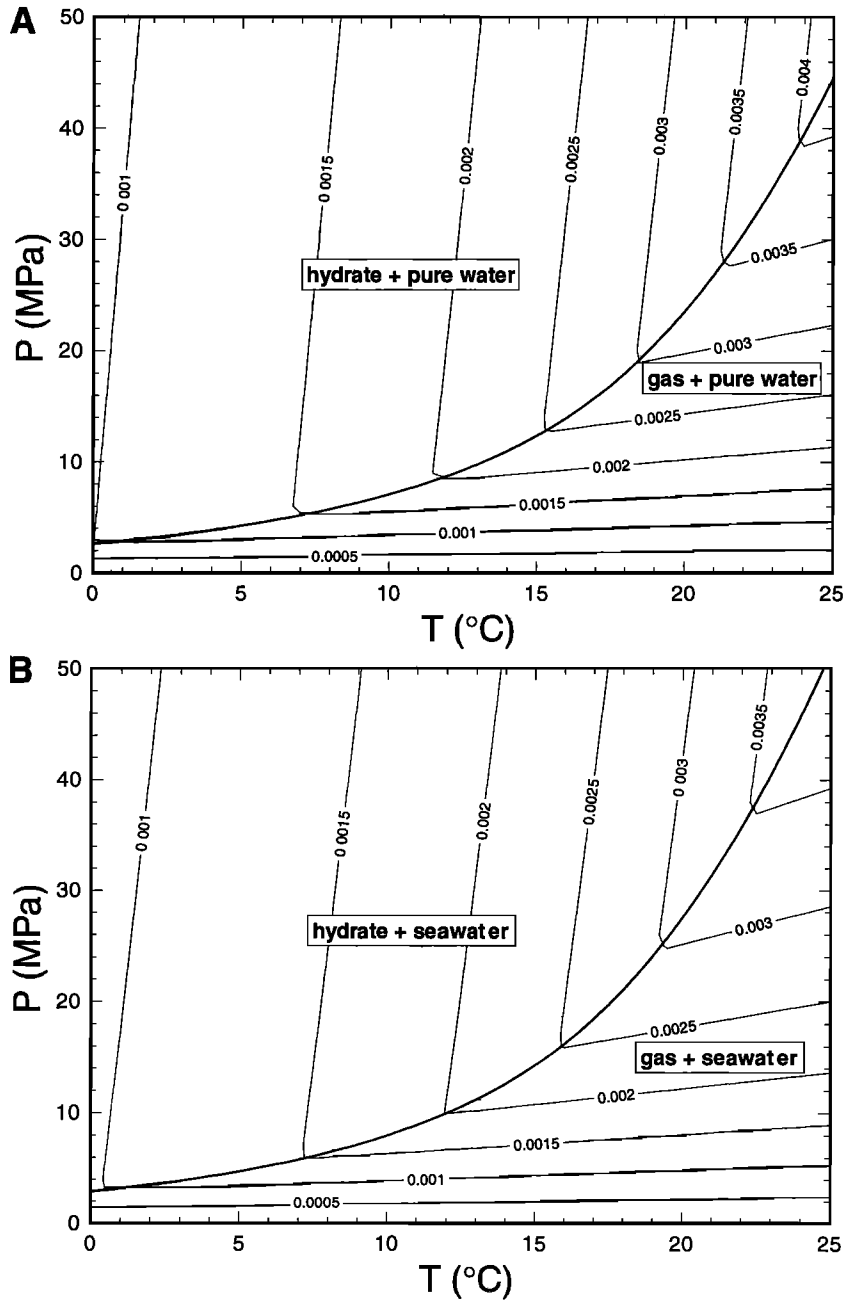

Figure 4. Equilibrium methane solubility in molar fraction computed for pure water and for seawater as a solvent.

3.2. Capillary Effects on the Gas Phase

Before considering capillary effects on the hydrate phase, we shall first examine the simpler case of the methane gas-water equilibrium. In pores, the water-gas interface takes a curved shape, concave on the gas side and surface tension increases the gas pressure P_g in the bubbles with respect to the pore fluid pressure P. This pressure increase (the capillary pressure) is given by the Young-Laplace equation [*Defay et al.*, 1966; *Washburn*, 1921]

$$P_g = P + 2\cos\theta\,\gamma_{gw}/r \qquad (2)$$

where r is the pore radius and θ is the wetting angle. The quantity γ_{gw} is surface energy (J m^{-2}). The wetting angle may also be understood from energetic considerations. Let γ_{gs} and γ_{ls} be the gas-solid and liquid-solid interfacial energies. Mechanical equilibrium of forces acting on the interface implies that $(\gamma_{gs} - \gamma_{ls}) = \cos\theta\,\gamma_{gw}$ [*Emschwiller*, 1961]. The variation of free energy when the surface of the solid-gas interface increases by dS at the expense of the liquid-solid interface is thus

$$dG = (\gamma_{gs} - \gamma_{ls})dS = \cos\theta\,\gamma_{gw}dS \qquad (3)$$

When free gas is present, fugacity of methane is computed from P_g as given by (2), with $\gamma_{gw} = 0.072$ J m^{-2} [*Tissot and Welte*, 1978]. It is assumed that the fluid is perfectly wetting ($\theta = 0°$ and $\cos\theta = 1$). This implies that a film of adsorbed water molecules actually covers all the mineral surfaces.

Equations (2) and (3) are, however, valid as long as the thickness of this liquid film (about 0.5 nm in the experiments with ice [*Handa et al.*, 1992]) is small compared to the pore size, and the pores are at least a few nanometers in size. The effect of (2) and (3) is to promote clathrate formation, through an increase in methane fugacity, wherever free gas exists in small bubbles, or is confined in pockets of high suface curvature within a porous medium.

3.3. Free Energy of Water in the Liquid Phase

In the marine subsurface sediment we may assume that the liquid phase pressure P is hydrostatic [*Hyndman and Davis*, 1992]. This assumption has important implications for the chemical potential of water in the sediment. Let us here consider an experiment in which a well is drilled and equipped with a perforated screen (so that water can be exchanged freely between the formation and the hole) and filled with fluid having the same composition as the pore fluid. If pore pressure is hydrostatic in the formation, the water in the well should be in equilibrium with the formation; therefore the chemical potential of water in the pore fluid should equal the chemical potential of water in the well. This virtual experiment shows that the chemical potential of water is not affected by adsorption on mineral surfaces if the system is assumed open for water. The validity of the open system assumption is, however, uncertain because this condition will depend on the time scale and length scale of the phenomenon considered and the transport properties of the sediment [*Clennell et al.*, this issue]. The assumption of hydrostatic pore pressure is mostly supported by considerations on permeability and sedimentation rate [*Hyndman and Davis*, 1992]. It may happen that the formation of hydrate occurs at a faster rate such that the assumption of an open system is no longer valid. In this case, pore pressure may locally become lower than hydrostatic. If water activity is defined from a reference state at hydrostatic pressure, water activity will decrease concurrently with pore pressure.

3.4. Capillary Effects on the Hydrate Phase

The model of *van der Waals and Platteeuw* [1959] for hydrate is based on the concept that gas molecules are adsorbed in rigid cages of water molecules that form the hydrate lattice. From this description, it may be thought that the contribution of the water lattice to the interaction between the hydrate and the surrounding liquid water is dominant and that the contribution of the gas molecules to the surface energy may be ignored. Laboratory experiments on hydrate in porous material do clearly establish that the thermodynamic properties of hydrates are dominated by those of water and indicate that cage occupancy is unaffected or only weakly influenced by surface effects [*Handa and Stupin*, 1992]. Consequently, we may correctly assume for a first-order approximation that the chemical potential of methane in the hydrate phase is not affected by surface effects. We will further assume that the surface energy of the hydrate-water interface does not depend on cage occupancy. With these assumptions, the effects of a restricted geometry may be treated considering the thermodynamic properties of a hypothetical empty hydrate lattice, as defined in the Appendix.

With appropriate assumptions and approximations, the behavior of crystalline solids in restricted geometries can often be described with the same approach as for fluids [*Defay et al.*, 1966]. We here assume that the surface energy of the hydrate water interface γ_{hw} does not depend on its orientation, that hydrate is incompressible, and ignore free energy terms that may arise from shear stress and strain. These approximations are valid for ice growing in pores [*Everett*, 1961; *Handa et al.*, 1992], and we assume that they are also valid for hydrate because of the structural similarity between ice and hydrate [*Clennell et al.*, this issue]. As demonstrated before, the chemical potential of water in the liquid phase is fixed, and independent of pore size, as long as the assumption of a hydrostatic pore pressure is valid. Equation (3) applied to the quantity of hydrate containing one mole of water then gives

$$(\mu_\beta - \mu_L) = (\mu_\beta - \mu_L)_{\text{bulk}} + V_\beta \frac{2\cos\theta\,\gamma_{hw}}{r} \qquad (4)$$

which is generally known as the Gibbs-Thomson equation. As defined in the Appendix, $(\mu_\beta - \mu_L)$ is the chemical potential difference between the empty hydrate lattice and liquid water, and V_β is, as previously defined, the molar volume of water in the hydrate lattice. If a layer of unfrozen water remains between the hydrate and the mineral surface, as is observed for ice [*Handa et al.*, 1992], hydrate may be considered as fully nonwetting and $\cos\theta=1$. Laboratory experiments show that thermodynamic properties of hydrate in small pores change the same way as those of ice [*Handa and Stupin*, 1992] implying similar interfacial energies for hydrate-water and ice-water. The interfacial energy of the hydrate-water interface will thus be assumed equal to that of a water-ice interface ($\gamma_{hw} = \gamma_{iw} = 0.027$ J m^{-2}) [*Clennell et al.*, this issue].

Handa and Stupin [1992] determined equilibrium conditions for methane hydrate in porous silica gel. The pore size distribution in this material determined by thermoporometry is almost Gaussian with a mean pore radius 70 Å and half width 40 Å and the corresponding decrease of the ice melting point is 5.7°C [*Handa et al.*, 1992]. The experimental conditions used (excess gas) imply that the pore hydrate rather than the pore water should be in equilibrium with the bulk phase. The free energy correction should thus be applied to the liquid and

$$(\mu_\beta - \mu_L) = (\mu_\beta - \mu_L)_{\text{bulk}} + V_L \frac{2\cos\theta\,\gamma_{hw}}{r} \qquad (5)$$

The experimentally determined gas pressures above 0°C fall near the hydrate-liquid-gas equilibrium curve computed for a pore radius of 7 nm, without parameter adjustments (Figure 5). The slope appears overestimated in our model either because the assumption of an equilibrium between pore hydrate and bulk hydrate is incorrect or because the effective pore size varies along the experimental curve. We conclude from this comparison that the effect predicted with the model has the correct order of magnitude at least for temperatures where experimental data exist.

3.5. Capillarity and Lithostatic Pressure

We have so far considered hydrate filling individual spherical pores or growing inside a rigid porous network, but hydrate may displace sedimentary grains to form segregated masses if this mode of growth is energetically advantageous (Figure 6) [see *Clennell et al.*, this issue]. In addition to capillary forces acting in the pores, the hydrate is in general subject to forces applied by the mineral grains with which it is in contact. Differential stresses are not supportable across hydrate-grain boundaries (assuming hydrate is fully

nonwetting) but pressures are. Locally, the pressure applied by a mineral grain will be balanced by the sum of the pressure in the hydrate near the contact and of the capillary pressure corresponding to the local surface curvature [*Clennell et al.*, this issue]. If able to deform, the hydrate mass will tend towards an equilibrium shape at uniform internal pressure P_i. This assumption is known as the "plastic ice" assumption [*Everett*, 1961], but if a continuous film of unfrozen water is present on the mineral surfaces, dissolution and recrystalization at the boundaries is a more likely deformation mechanism than plasticity. The nature of the process by which the internal pressure equilibrates is, however, unimportant for our purpose, which is to compute the equilibrium conditions. The assumption of rigid cages implies that the chemical potential of the methane adsorbed in the cages does not depend on P_i (see Appendix). Applying then the Gibbs-Duhem equation to the hydrate, the free energy difference between the empty hydrate lattice at pressure P_i and water at hydrostatic pressure is the quantity we require:

$$(\mu_\beta - \mu_L) = (\mu_\beta - \mu_L)(P_{hydr}) + V_\beta (P_i - P_{hydr}) \quad (6)$$

If a characteristic pore radius r can be defined, the combination of (6) and (4) implies

$$P_i = P_{hydr} + 2\cos\theta\, \gamma_{hw}/r \quad (7)$$

Equation (7) may also be found more directly by applying the Young-Laplace equation (2) to the hydrate phase. We chose the more progressive approach above to provide a more detailed explanation of the assumptions involved. Again assuming $\cos\theta = 1$, the capillary pressure is $P_c = 2\gamma_{hw}/r$ (Figure 6A).

A body of hydrate may be considered as a segregated mass if it has evolved into a simple shape, either nodule or lens, that does not include many sediment grains, and if it is large compared to the sediment grain size. In terms of thermodynamics the mass will effectively assume bulk properties when it is large enough that its surface energy may be neglected. With this definition, a spheroid of 100 μm radius in a clay matrix may actually qualify as a segregated mass. We will not attempt to compute the equilibrium shape for such an inclusion but simply remark that the internal pressure shall be bounded by the minimum and maximum principal stresses (σ_3 and σ_1) in the formation. For sediments undergoing burial in nontectonic environments and under hydrostatic pore pressure, the stress state may be estimated as

$$\sigma_1 = P_{lith} \quad (8a)$$

$$\sigma_3 = P_{hydr} + K_0 (P_{lith} - P_{hydr}) \quad (8b)$$

where K_0 is about 0.5 for shale and mudstone for a wide range of applied stresses [*Karig and Hou*, 1992; *Jones*, 1994]. The internal pressure P_i of the segregated hydrate should thus be bounded by

$$0.5(P_{lith} - P_{hydr}) < (P_i - P_{hydr}) < (P_{lith} - P_{hydr}) \quad (9)$$

These bounds are shown on Figure 6 for a typical deep marine sedimentary basin with an exponential distribution of

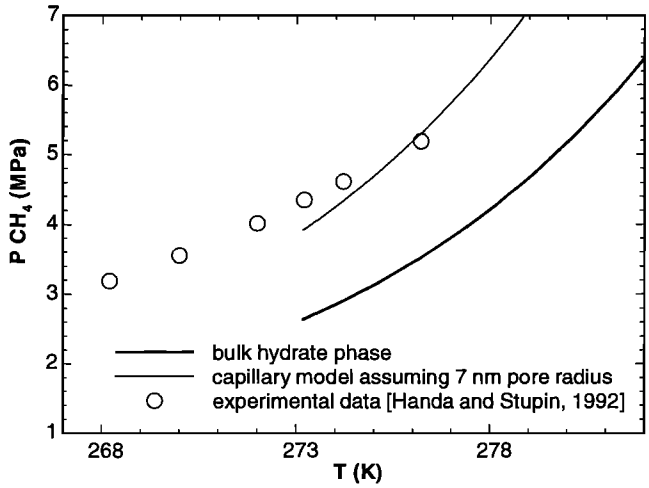

Figure 5. Computations with the capillary model are compared with data for the hydrate-liquid water-gas equilibrium in 70-Å-radius-pores silica gel [*Handa and Stupin*, 1992].

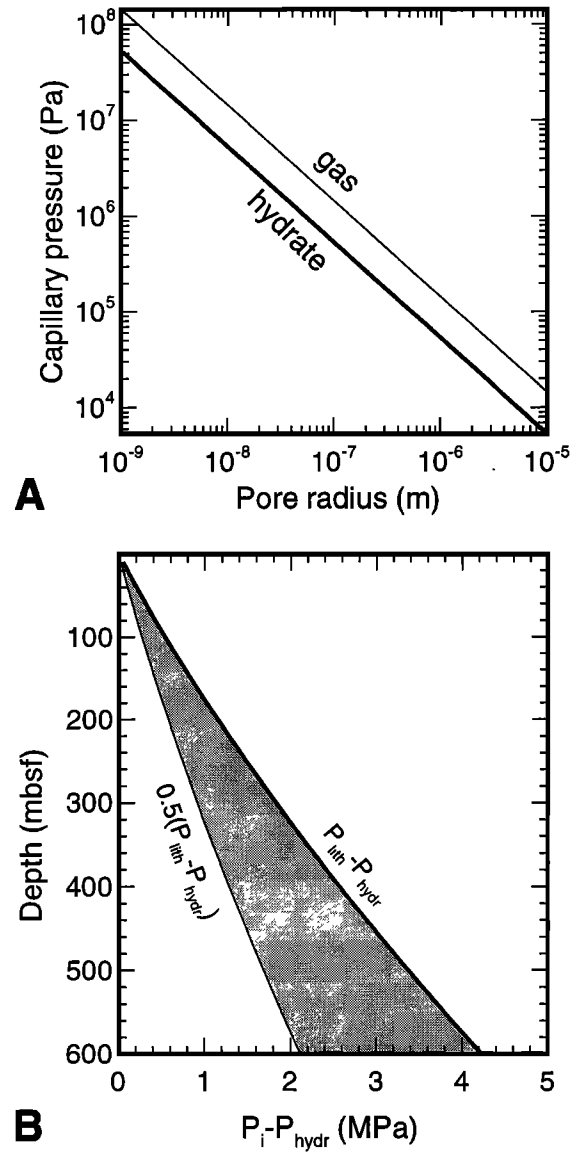

Figure 6. (a) Relationship between pore radius and capillary pressure for interstitial hydrate and gas. (b) Upper and lower bounds for the excess internal pressure (P_i -P_{hydr}) in segregated hydrate masses for a typical deep sea sedimentary basin with porosity, $\varphi = 0.7 \exp(-z/1500)$ [*Le Pichon et al.*, 1990], with depth z in meters and with a grain density of 2700 kg m^{-3}. Theoretically, hydrate should take the habit (segregated or interstitial) which minimizes its internal pressure.

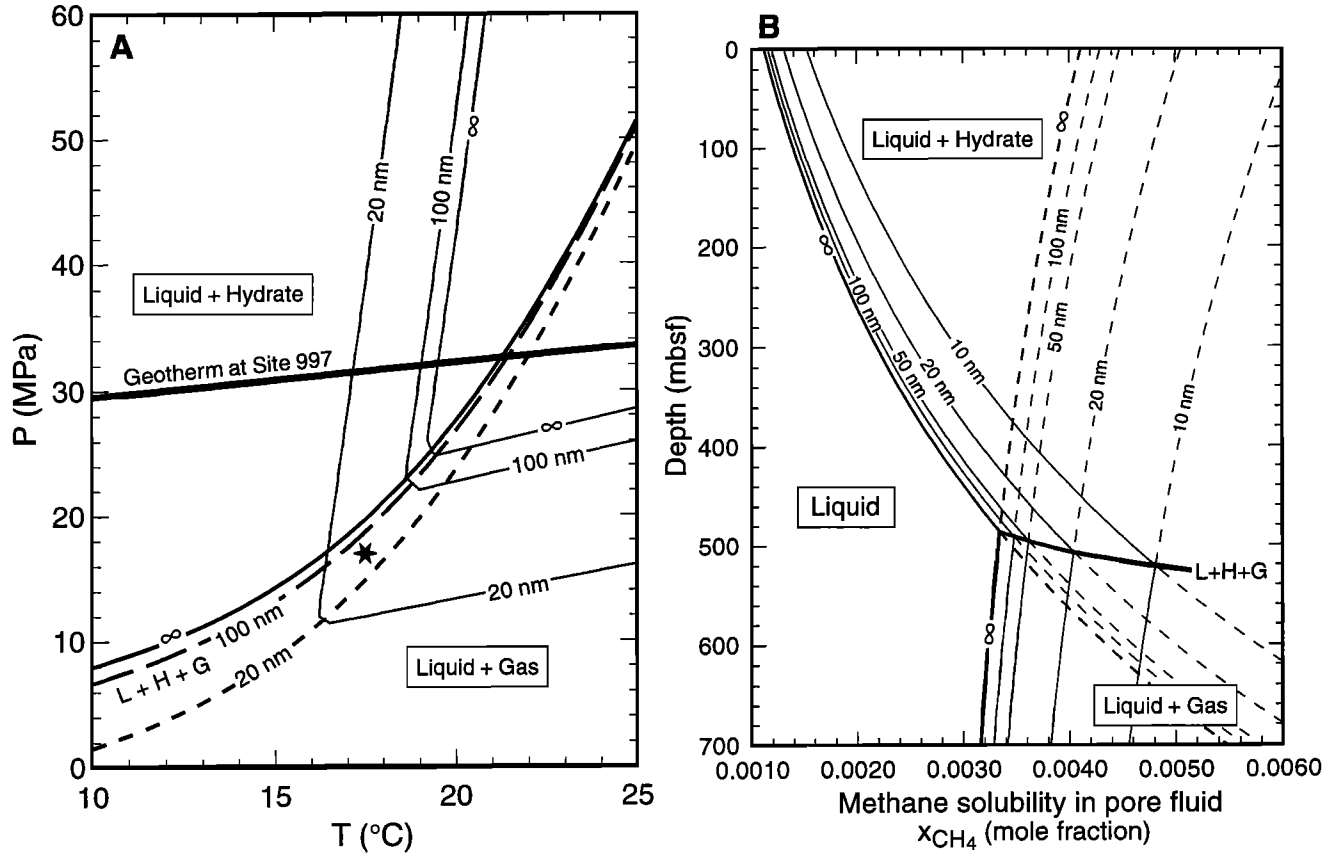

Figure 7. Effect of pore size on methane solubility and on the hydrate+water+gas equilibrium. (A) equilibrium P,T conditions assuming the same effective pore size for the gas and for the hydrate phase. Methane solubility curves are given for mole fraction $x_{CH_4} = 0.003$. For the pressure conditions indicated by the star (17 MPa and 17.5°C) water+gas is stable for pores larger than about 50 nm, whereas water+hydrate is stable for pores smaller than about 50 nm. The geotherm at Blake Ridge Site 997 is given as an example. (B) methane solubility as a function of depth for Site 997 geotherm. All computations are performed for seawater with 30‰ salinity.

porosity with depth [*Bray and Karig*, 1985; *Le Pichon et al.*, 1990]. Consequently, segregated hydrate and interstitial hydrate may coexist if

$$0.5(P_{\text{lith}} - P_{\text{hydr}}) < P_c < (P_{\text{lith}} - P_{\text{hydr}}) \quad (10)$$

and hydrate growing in pores should not segregate if pores with radius

$$r > 4\gamma_{hw}/(P_{\text{lith}} - P_{\text{hydr}}) \quad (11)$$

are accessible.

4. Results of Computations for a Single Pore Size

4.1. Solubility Limits

Before considering the case of a real sediment with a broad distribution of pore sizes, we treat the case of a porous network characterized by a single pore size. The primary effect of capillarity is to increase the solubility of methane in the pore water, both with respect to the free gas phase and to the hydrate phase. In Figure 7, methane solubility curves for various pore sizes are shown in the pressure-temperature space and as a function of depth for the geotherm at Blake Ridge Site 997. This example may be considered as a typical case.

On the *P,T* diagram, a concentration of 0.003 mole fraction was chosen only for the purpose of graphic representation, so that the solubility limits can be seen clearly and is not meant to represent the expected methane concentration in hydrate bearing sediments. The total methane content measured using the pressure core sampler (PCS) near the level of the BSR at Blake Ridge Sites 995 and 997 is 3 to 10 times larger than this value [*Dickens et al.*, 1997b]. Therefore the interpretation of the BSR as a transition from methane hydrate to methane gas is valid; there is enough methane present in the system for a separate methane rich phase to coexist with methane dissolved in the pore water. It is possible that at other locations (such as at Site 994) the top of the gas and the base of the hydrate do not coincide and are instead separated by a zone where all the methane stays in aqueous solution. This is because methane reaches a maximum of solubility at the three phase equilibrium and this may occur even if capillary effects are not considered (Figure 7). Capillary effects would, however, widen the zone containing just the aqueous phase for a given methane concentration in the system, for the simple reason that there is an energy penalty associated with creation of new phase interfaces (gas-water or hydrate-water) and this becomes significant in small pores.

4.2. Behavior of the Three-Phase Equilibrium

Our first and most important result is that several outcomes are possible depending on the configurations that we assume the hydrate, gas, and water adopt. Combining capillary effects on gas and hydrate phases, a slight increase of the stability of hydrate relative to methane gas is obtained. For example, at 17 MPa and 17.5°C (star on Figure 7) water+gas is stable for pores larger than about 50 nm, whereas water+hydrate is stable for pores smaller than about 50 nm. This would imply a downward shift of the BSR compared with the bulk phase equilibrium. Consequently, capillary effects at equilibrium cannot be invoked to explain observations of BSR at a shallower depth than predicted with bulk phase equilibrium, unless one assumes that capillary effects only act on the hydrate phase and not on the gas phase. Indeed, it may be thought that in real sediments, which have a wide distribution of pore sizes, the pore size relevant for the gas is not in general equal to the pore size relevant for the hydrate. As shown on Figure 7, the three-phase equilibrium may be shifted upward or downward if different pore sizes, or at least equivalent values of mean interfacial curvature, are assumed for hydrate and gas inclusions. We shall reexamine this possibility later in the light of pore size data.

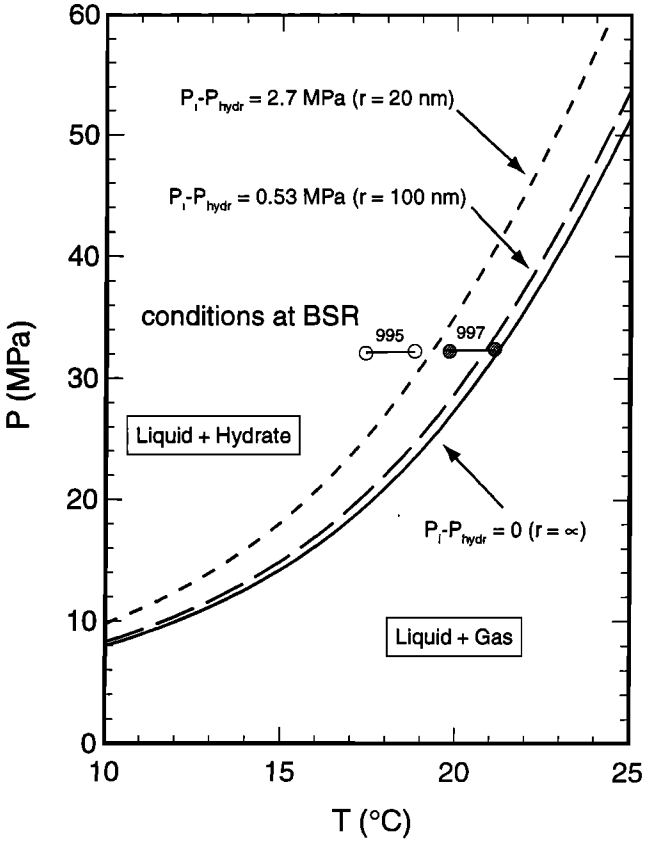

Figure 8. Effect of internal hydrate pressure on the hydrate+water+gas equilibrium, ignoring capillary effects on the gas phase. Internal pressure may either result from the sedimentary load on segregated hydrate or from capillary effects on interstitial hydrate. The corresponding pore size is given. Computations are performed for seawater with 30‰ salinity. Upper and lower temperature and pressure bounds from ODP drilling Sites 995 and 997 on Blake Ridge are also indicated. At Site 995 the pore size required for a correct prediction of the three-phases equilibrium would be 10-20 nm.

Alternatively, application of a confining pressure on segregated hydrate masses may cause an upward shift of the base of the hydrate stability field (assuming hydrostatic pore pressure). In the absence of sufficiently detailed in situ observations it is impossible to distinguish true interstitial hydrate (subject to fluid pressure only) from small segregated hydrate inclusions (subject to a pressure intermediate between hydrostatic and lithostatic). The excess lithostatic pressure (P_{lith} - P_{hydr}) at the BSR depth on Blake Ridge is about 3.5 MPa (with an average bulk density of 1.8 kg m^{-2}), implying internal pressures of 1.8 to 3.5 MPa in a segregated hydrate mass (Figure 6). The internal pressure thus equals the capillary pressure for a pore radius of 15 to 30 nm (Figure 6) and would cause a shift of 1.5° to 3°C of the hydrate dissociation curve towards a lower temperature (Figure 8), ignoring the capillary effect on the gas phase. This explanation is not very satisfactory because one may expect the hydrate to first form in larger pores and segregate only when pores with an access radius of more than 15-30 nm are no longer available [*Clennell et al.*, this issue]. We will also come back to this point after characterization of the pore size distribution.

5. Application to Sediments With a Broad Pore Size Distribution

5.1. Significance of Mercury Porosimetry Tests

Because mercury is a nonwetting fluid, mercury porosimetry may be equivalent, under certain conditions that we shall define, to the growth of interstitial hydrate or of gas bubbles in sediment. During porosimetry tests, mercury is injected quasistatically (such that viscosity effects are negligible) at a progressively increasing pressure into a dried and evacuated sample [*Arnould et al.*, 1980; *Lowell and Shields*, 1984]. A retraction curve may also be obtained by reversing the process. Assuming the sample has been properly evacuated, mercury pressure is the capillary pressure in the smallest pore throats which the mercury can enter and thus follows the Young-Laplace equation

$$P_{Hg} = - 2 \cos\theta \gamma_{Hg}/r \qquad (12)$$

with parameters $\theta = 140°$ and $\gamma_{Hg} = 0.485$ J m^{-2}. The volume filled by the mercury at a given pressure thus represents the pores that can be accessed from the surface of the sample through pore throats larger than a given radius. Consequently, the inflection point of the phase fraction (phase fraction is defined as the fraction of the pores occupied by a phase) versus pressure curve represents a percolation threshold rather than a peak in the actual pore size distribution [*Katz and Thompson*, 1987]. When the pressure is brought back to zero, some mercury stays trapped in pores that are only connected to the surface through smaller throats, so that the intrusion curve is not retraced: an effect called geometrical or network hysteresis [*Pellerin*, 1980; *Portsmouth and Gladden*, 1991]. Assuming the porous framework is rigid, the same behavior is expected if gas is injected into a water-saturated sample. For spontaneous growth of gas bubbles or hydrate in sediment with supersaturated pore fluid, the constraint that bubbles (or hydrate) must be connected to the surface is removed. Below the percolation threshold, the capillary pressure should thus be lower than for the hypothetical gas injection case at the same phase fraction but both should be equal above the

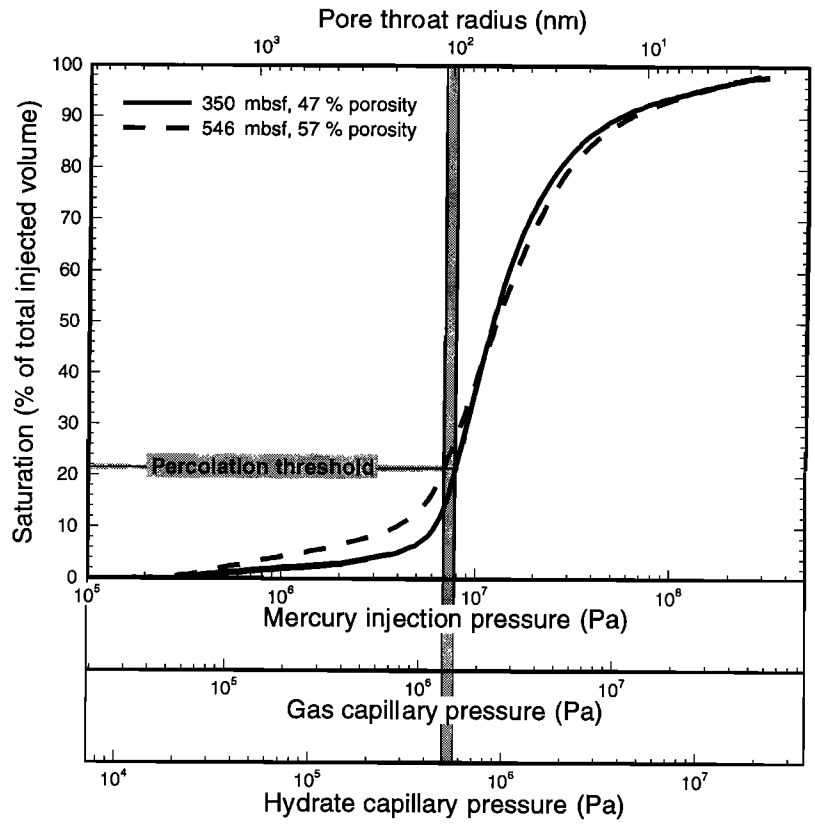

Figure 9. Mercury injection tests on samples from Blake Ridge ODP Hole 995A, taken 100 m above (at 350 mbsf) and 100 m below (at 546 mbsf) the BSR. The total porosities of the samples are 47% (at 350 mbsf) and 57% (at 546 mbsf). The percolation threshold (see text) corresponds to the inflection point of the phase fraction versus pressure curve. Mercury pressure and pore throat radius are indicated as well as the corresponding capillary pressures for gas and hydrate.

percolation threshold. For an order of magnitude approximation, we assume that the capillary pressure for gas and hydrate can be directly derived from the mercury injection test by using the appropriate surface energies (γ) and wetting angles (θ).

5.2. Mercury Porosimetry Results

Two samples from Blake Ridge drill hole 995A were analyzed (Figure 9). They have similar lithology and were taken 100 m above (at 350 mbsf) and 100 m below (at 546 mbsf) the BSR. Unexpectedly, the deeper sample has a larger total porosity (57%) than the shallower one (47%). This difference in porosity does not reflect a trend of increasing porosity with depth (average porosity is practically constant below 300 mbsf) but is representative of the measured porosity fluctuations [*Paull et al.*, 1996]. The percolation threshold (maximum of dV/dP) is the same (20-22%) for both samples and corresponds to a pore size of 100 nm. The shape of the porosimetry curves are similar above the percolation threshold (for small pores) but the fraction of pores with large access radii (more that 200 nm) is larger in the more porous sample.

5.3. Predictions and Constraints Deduced From the Specified Pore Size Distribution

The hydrate phase fraction (fraction in the pore space S_h) in Blake Ridge sediments has been estimated from the pore fluid chlorinity anomalies and from resistivity logs and never exceeds 23%, even in the most hydrate rich horizons. S_h determined from resistivity logs have "background" values of 5.8% at Site 994, 7.9% at Site 995, and 7.6% at Site 997 in the depth range of approximately 190-400 mbsf but tend to increase immediately above the BSR, up to 11.6% at Site 995 and up to 19% at Site 997 [*Paull et al.*, 1996]. As mentioned earlier, gas phase fraction reaches 12% immediately below the BSR at Site 997 but should be lower elsewhere. These values place both free gas and hydrate phase fractions below the percolation threshold expected for these sediments. The effective pore throat radius that hydrate can penetrate at these phase fractions will always be more than about 100 nm, corresponding to a hydrate capillary pressure less than 0.5 MPa. If the mercury injection tests are representative, the observed BSR shift of 2-3°C at Site 995 cannot be explained by a modification of the thermodynamic equilibrium arising from capillary effects for any values of S_h and S_g in the observed range. It is also unlikely that the hydrate will segregate at the depth of the BSR in Blake Ridge, as capillary pressure would be less than 1/5 of the lithostatic pressure.

Let us first consider separately the hydrate+water and hydrate+gas two-phase equilibria. We have seen that the concentration of methane in a solution in equilibrium with either hydrate or gas is a function of pore size. The relationship between methane concentration in the pore fluid and phase fraction (Figure 10) is computed assuming that the phase fraction versus pore size curve is the same for mercury

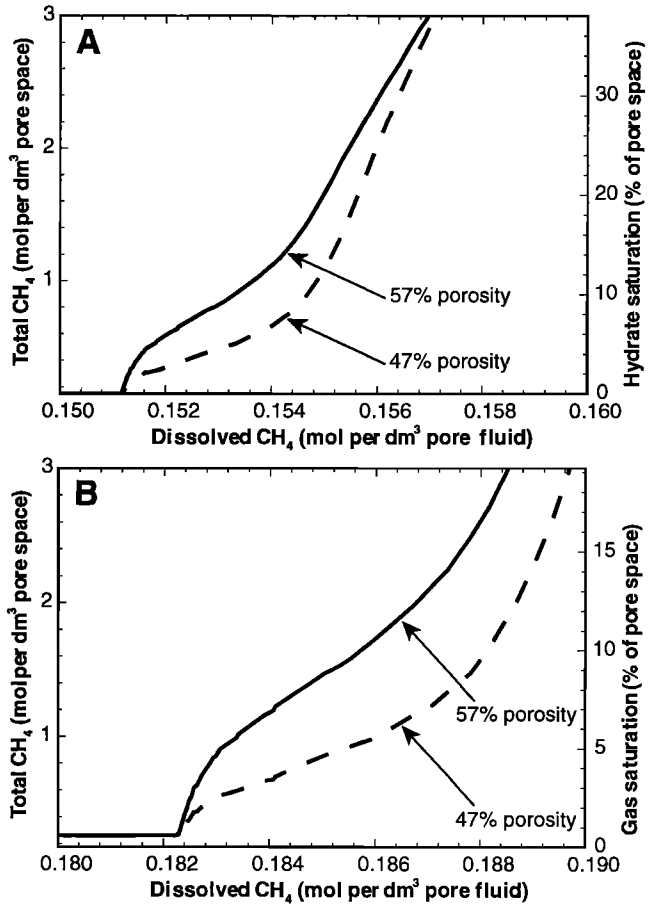

Figure 10. Phase fraction and total methane content as a function of equilibrium methane concentration in the pore fluid: (a) for hydrate-water equilibrium and (b) for free gas-water equilibrium. Curves are based on mercury porosimetry data obtained below the percolation threshold (Figure 4) and thus are approximate. At the location of the arrows, hydrate or gas phase fraction is about twice larger in the more porous sample for the same concentration of methane in solution.

injection as for the growth of hydrate or of gas bubbles. The total methane content per pore space volume is derived from this relationship and the molar volumes of the phases. At the pressure and temperature condition at BSR depth on Blake Ridge (32.5 MPa, assuming a 10 MPa km^{-1} hydrostatic gradient [*Paull et al.*, 1996] and about 20°C [*Ruppel*, 1997]) the molar volume of the gas phase is about 68.6 cm^3 from the virial EOS [*Duan et al.*, 1992] and the volume of hydrate containing one mole of methane is 131.4 cm^3 (with V_β = 22.5 cm^3 [*Handa*, 1990] and n = 5.84 from this study). For a given methane concentration in the pore fluid, the hydrate or gas content in the sediment is expected to be about twice as large in the more porous sample (Figure 10) because it has a greater proportion of large pores than the less porous sample. This example suggests that the moderate fluctuations in porosity, grain size and packing density that often occur within a few meters in apparently homogeneous formations may strongly affect the ability of the sediment to host hydrate or gas. If molecular diffusion homogenizes the concentrations of dissolved methane at the 1-30 m scale, the observed small-scale variations of hydrate content could just reflect variations in the pore size distribution and may correlate with porosity or other physical properties such as grain size.

5.4. Three-Phase Equilibrium When Phase Fraction is an Additional System Variable

A consequence of the progressive rise of methane solubility with gas or hydrate phase fraction is that the three phases may coexist over a range of depths (Figure 11) according to methane content and pore size distribution. The upper limit corresponds to the case when gas is present in such small quantities that capillary effects may be neglected, that is, only very large pores are occupied by gas and hydrate, which consequently have low capillary pressures and thermodynamic properties similar to the bulk. The lower depth limit corresponds to the case when capillary effects on the hydrate phase may be neglected. The three phase zone widens with increasing total methane content, as higher capillary pressures are experienced. With the parameters for Blake Ridge Site 997 and knowing that the maximum measured total methane concentration is 2 mol per dm^3 of pore space (corresponding to 12% gas phase fraction or 25% hydrate phase fraction) the maximum width of this zone is about 25 m. We note that such a system will have hysteresis, as the phase initially present will occupy the large pores. Therefore the hydrate+liquid+gas should be interpreted as a zone where the three phases may be present rather than a zone where the three phases have to be present and the transition between hydrate and gas may occur more abruptly [*Clennell et al.*, this issue].

6. Discussion

The pore size data we obtained from Blake Ridge samples are very limited, yet the pore size distributions are compatible with what we know of the sediment mineralogy and microstructure seen with electron microscopy and from unpublished nuclear magnetic resonance data. Our mercury porosimetry curves are also comparable with curves for similar sediments (M.B. Clennell, unpublished data, 1997) and with data on compacted silty clays published elsewhere [*Griffiths and Joshi*, 1991, and references therein]. If the investigation of pore size distribution by mercury porosimetry is relevant for hydrate, capillary effects in the Blake Ridge sediments may only shift the temperature at the base of the hydrate stability field by a fraction of 1°C, relative to the bulk phase equilibrium. Figure 8 shows the maximum shift towards a lower temperature of the hydrate+gas+seawater equilibrium for effective pore sizes 20 and 100 nm. This maximum shift has been computed neglecting capillary effects in the gas phase and may correspond to a case with low gas phase fraction beneath the BSR. Considering the uncertainties on both BSR depth and geotherm, it appears that Site 997 may in fact be compatible with the equilibrium predictions, but Site 995 clearly lies outside the acceptable range.

Even if our computations of the capillary effect fail to explain the temperature data at Blake Ridge, the lack of experimental data on the conditions for hydrate stability in fine-grained sediments prevents us from drawing a final conclusion. A number of the assumptions made in the model may also be wrong; we are now able to assess some of these quantitatively and provide some useful constraints.

1. The surface energy of the hydrate-water interface may have been underestimated, but it is not possible to increase it

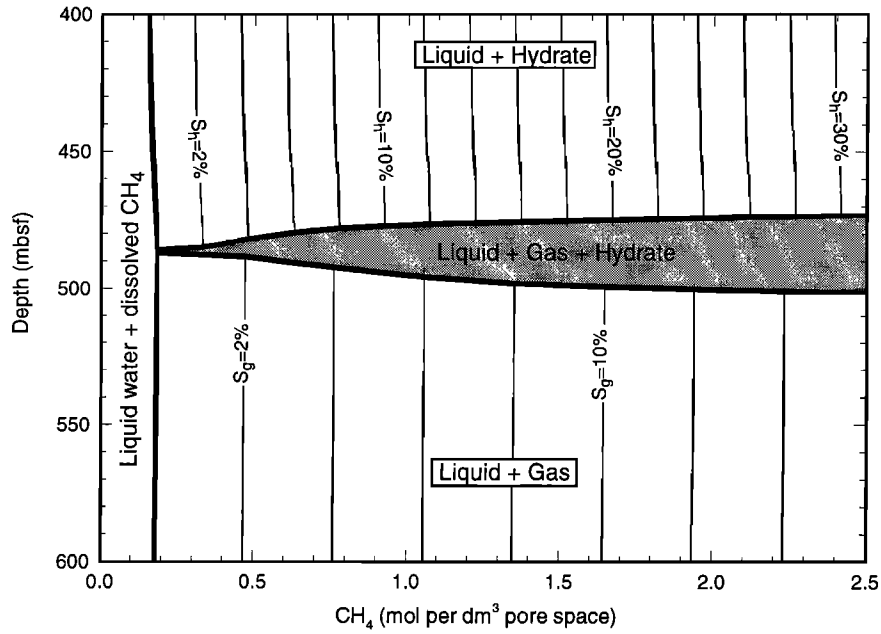

Figure 11. Phase stability diagram computed for the geotherm at Blake Ridge Site 997. The limits of the zone where hydrate, seawater, and methane gas may coexist is based on mercury porosimetry data from the least porous sample (47% porosity and 350 mbsf). This choice maximizes capillary effects. Note that for the highest measured total methane concentration (2 mol per dm^3 pore space) the width of the three-phase zone is only about 25 m. In the two-phase regions, hydrate or gas phase fraction is given.

significantly and still fit the data of *Handa and Stupin* [1992]. Changing the wetting angle would decrease capillary effects for a given pore size and thus would not help explaining the observed BSR shift.

2. If water cannot be exchanged freely though the porous network, the activity of water may become lower than that in the bulk pore fluid due to water adsorption on surfaces. This effect is equivalent to that of lowering pore fluid pressure below hydrostatic pressure. For the 17.4°-18.7°C temperature at Blake Ridge Site 995, a pore pressure of about 25 MPa would be required to bring the estimated *P,T* conditions at BSR depth on the three-phase equilibrium curve. This pressure is lower than the 27.7 MPa hydrostatic pressure at the seafloor.

3. The capillary model may be inappropriate for very small pores. The mercury injection tests, however, identify a population of relatively large pores (> 100 nm) in which the capillary approach is most probably valid. If hydrate or gas are able to form in these pores, capillary effects will be small. Note that the presence of an electric double layer around clay minerals does not significantly reduce the pore sizes because this layer is only about 0.6 nm thick in seawater [*Revil and Glover*, 1997; *Henry*, 1998].

4. The system may not be at equilibrium but controlled in part by the kinetics of hydrate nucleation and growth. Furthermore, nucleation of methane hydrate could be inhibited in small pores [*Clennell et al.*, this issue]. If kinetic effects are important, the equilibrium model would underestimate the supersaturation of methane in the pore fluid and the width of the zone where gas and hydrate may coexist. Given a solution supersaturated with respect to both gas and hydrate, gas bubbles would be observed instead of hydrate if they are able to grow out of methane in solution faster than the hydrate.

5. We should also allow for possible perturbation of the equilibrium state of the system in the presence of a dynamic flux of fluids and heat, as proposed by *Rempel and Buffett* [1997] and modeled for a typical submarine system by *Xu and Ruppel* [1999]. We cannot discuss the relative merits of different models here but note that the "continuum" and "pore scale" approaches are complementary. Indeed, the capillary effects we describe in our model will be additive to any global perturbations in *P,T* structure caused by directed flow. Furthermore, the low-permeability, high-capillary entry pressure and percolation properties constrain the possible rates and mechanisms of gas transport in dynamic systems. Where petrophysical data are available, our approach can be used to identify not only preferred sites of hydrate growth but also, within bounds, the amounts that will be precipitated.

Inhibition of nucleation, possibly in combination with kinetic effects, appears to us as the most promising explanation of the shifted phase boundaries at Blake Ridge. Surface effects are an important factor in nucleation processes, and pore size should play a role as it will limit the size of nuclei. The equilibrium capillary model presented here could still be useful in this context as it gives the critical radius of hydrate and gas nuclei for a given methane concentration in the pore fluid.

7. Conclusion

Both free gas and hydrate are subject to capillary forces but with opposite effects on hydrate stability. Displacement of the equilibrium conditions thus depends on the fraction of pore space filled by hydrate and by gas, and any tendency of a particular phase to occupy the larger pores. Bottom-simulating reflectors which represent the gas+hydrate+water equilibrium may be shifted upward (towards a lower temperature) or downward (toward a higher temperature) relative to bulk phase equilibrium depending on the respective

hydrate and gas content of the sediment. Lateral variations of the temperature of the BSR may thus correlate with the amount of gas present immediately below the BSR, but the minimum pore size (30-60 nm) required to explain the vertical offset between drill holes at Blake Ridge is probably too small, and uncompatible with porosimetry data.

It is possible that pore size effects can only be observed at a high free gas or hydrate phase fraction. Capillary theory calls for the existence of a percolation threshold for nonwetting phases in a porous medium. Below the percolation threshold, hydrate masses and bubbles are discontinuous, filling only the larger pores. Above the percolation threshold, hydrate or gas are continuous throughout the porous network. This transition probably has to be taken into account in models for physical properties of hydrated sediment. The pore throat size at percolation threshold (about 100 nm for Blake Ridge sediments) is likely to determine the conditions for the migration of free gas and the conditions under which hydrate grows as an interstitial or as a segregated phase. Measured hydrate and phase concentrations of methane in Blake Ridge generally lies below the percolation threshold for hydrate or gas, which implies that capillary effects cause only a small equilibrium displacement with respect to the bulk phase equilibrium.

A number of field observations may still be explicable by capillary effects.

1. Anomalies in the distribution of gas hydrates with depth. In the clay matrix supported sediments at Blake Ridge, hydrate concentration appears greater in sediments that contain more coarse silt [*Ginsburg et al.*, 1999] or that contain large (10 μm radius or more) shelter pores such as microfossils [*Kraemer et al.*, 1999].

2. The hydrate blanking effect. The decrease of sediment reflectivity within the hydrate zone may be explained if local variations of seismic velocity caused by local variations of hydrate content compensate those caused by local porosity changes [*Lee et al.*, 1993]. Capillary effects could cause this compensation to occur even at small hydrate contents (5-10%). If porosity differences in an homogeneous formation reflect differences in the number of large pores, layers of higher porosity would proportionally host more hydrate and have a proportionally increased seismic velocity. The intensification of sedimentary reflectors in the gas zone may be explained applying a similar reasoning to the gas phase (gas decreases seismic velocity).

3. Distribution of hydrate between interstitial hydrate and segregated masses. Unsheltered masses of hydrate are subject to pressures intermediate between hydrostatic and lithostatic. At shallow depths, this effect is small and hydrate preferentially grows as segregated masses rather than in small pores. At the depth of the BSR on Blake Ridge (450 m) the effect of the confining pressure is larger than the expected capillary effects and hydrate is expected to be interstitial. With the assumptions made (equilibrium methane concentration in solution and stress conditions that are not valid for a fault zone), the maximum depth at which hydrate may segregate is 160 m in the Blake Ridge case (for a pore size of 100 nm at the percolation threshold). It is important to note that the capillary-induced segregation process that we consider is valid for a fluid and thus also applies to gas. If this does occur for gas, the sediment will evolve into a mud mousse. This process may play a role in slope instabilities.

4. Mobile or static gas. As long as the pore fraction filled by free gas stays below a percolation threshold (estimated as 21-22%) gas bubbles are expected to stay trapped by capillary forces, and gas transport would occur by diffusion in the aqueous phase or by advection of dissolved gas with the aqueous phase. Therefore there may be no need to invoke a hydrate seal to explain moderate gas accumulations (up to 20 % phase fraction). Alternatively, the capillary effect may enhance the capability of hydrate to block gas migration because hydrate and gas will compete for the largest pores. Hydrate present immediately above the BSR should block the migration of gas bubbles much more efficiently than the migration of the liquid phase but should not be considered as a barrier for diffusion because diffusion is fairly insensitive to pore size.

Appendix

A1. Principles of Hydrate Thermodynamic Models

Models used to predict the stability of gas hydrates use a combination of classical and statistical thermodynamics [*Bishnoi et al.*, 1989, *Holder et al.*, 1988, *Munck et al.*, 1988, *Tohidi et al.*, 1995, *Van der Waals and Platteeuw*, 1959] and are derived from the model of *Van der Waals and Platteeuw* [1959]. These models can handle gas mixtures, but here we only consider cases with a single hydrate forming gas, methane, and assume that it is the only constituent of the gas phase if a gas phase is present. As in the natural case, water is assumed to be present as a liquid phase but its activity may not be 1. The basic assumptions underlying the statistical thermodynamic model and subsequent derivations are detailed by *Holder et al.* [1988] and by *Sloan* [1990]. The chemical potential of water in the hydrate phase μ_H is expressed as a function of the probability η_i that a cavity of type i is occupied by a gas molecule:

$$\mu_H = \mu_\beta + RT\sum_i \nu_i \ln(1-\eta_i) \qquad \text{(A1)}$$

where i refers to the cavity type (i = 1 or 2 for type I hydrate), ν_i is the number of cavities of type i per molecule of water and μ_β is the chemical potential of water in a hypothetical empty lattice state. The occupancy of the cages is related to the fugacity of methane by the Langmuir constants C_i:

$$\eta_i = C_i f/(1+C_i f) \qquad \text{(A2)}$$

The Langmuir constants are computed as a function of the temperature with no pressure dependency. It follows that (μ_H-μ_β) only depends on methane fugacity and temperature. The condition for equilibrium with water in a liquid phase at chemical potential μ_L is

$$\mu_H - \mu_L = (\mu_\beta - \mu_L)(T,P) + RT\sum_i \nu_i \ln(1-\eta_i) = 0 \qquad \text{(A3)}$$

(μ_β-μ_L) is computed from classical thermodynamics formula [*Holder et al.*, 1988]:

$$\frac{\mu_\beta - \mu_L}{RT}(P,T) = \frac{\mu_\beta - \mu_L}{RT}(0,T_0) - \int_{T_0}^{T}\frac{(H_\beta - H_L)}{RT^2}dT + \int_0^P \frac{(V_\beta - V_L)}{RT}dP - \ln a_w \qquad \text{(A4)}$$

where, as above, β refers to the empty hydrate frame and L refers to water in the liquid phase; a_w is the activity of water. The influence of dissolved methane on water activity is ignored, thus $a_w = 1$ for pure water as a solvent.

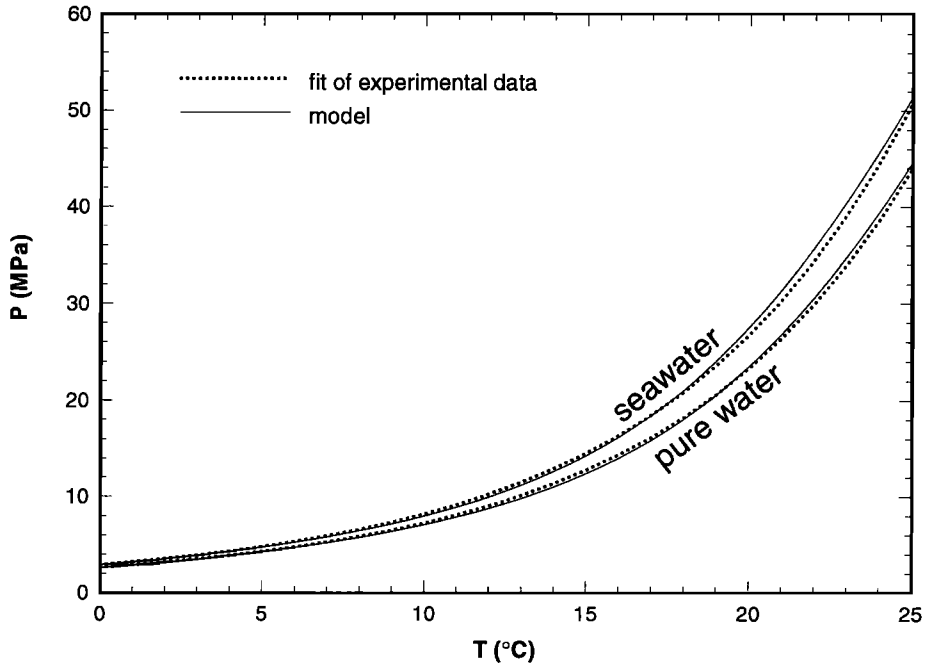

Figure A1. Hydrate+liquid+gas equilibrium plotted for pure water and seawater. Fits of experimental data are from *Handa* [1990] for pure water and from *Dickens and Quinby-Hunt* [1997] for seawater.

A2. Implementation for the Methane Hydrate–Water System.

The computations at a given pressure and temperature are performed in three independent tasks: (1) computation of methane fugacity for a given equilibrium gas pressure or a given concentration in solution, (2) Computation of Langmuir constants and (3) Computation of $(\mu_\beta - \mu_L)$.

The computation of the methane fugacity requires a volumetrically precise EOS, combined with an accurate model of methane solubility. The model of *Duan et al.* [1992] is well adapted to the problem of hydrates in marine sediments as it takes into account the effect of dissolved salts and gives an accurate partial volume for methane in solution.

Parameters from *Munck et al.* [1988] are used for the computation of the Langmuir constants and for $(\mu_\beta - \mu_L)$. The variation of enthalpy difference with temperature is approximated assuming a constant heat capacity difference.

Different cases have to be considered depending of the P,T conditions. In the water+gas domain, the fugacity and methane solubility are simply given by the methane EOS and the solubility model. In the water+hydrate domain, $(\mu_\beta - \mu_L)$ is first determined. The equilibrium methane fugacity is then computed from (A3) and from the Langmuir constants. The equilibrium methane solubility is then computed from the methane solubility model. The three-phase equilibrium is obtained as the intersection of the saturation curves for the hydrate+water and gas+water systems. The consistency of the model was checked by comparing the three-phase equilibrium curve with a fit of experimental data [*Handa*, 1990]. Because the model of *Munck et al.* [1988] used SRK equation, changing the methane EOS to a virial one caused imprecision: temperatures predicted for the hydrate+pure water+gas equilibrium were 0.5° to 1°C too low at high pressure (20-50 MPa). The Langmuir constants are fitted parameters in the model of *Munck et al.* [1988] and a better fit (±0.2°C) is obtained by increasing the Langmuir constants by 1.5% at all temperatures (Figure A1). After this correction, the values of cage occupancy obtained at 0°C are closer to published values: $\eta_1 = 0.886$, $\eta_2 = 0.973$ and $\eta_1/\eta_2 = 0.91$, to be compared with $\eta_1 = 0.893$, $\eta_2 = 0.975$ and $\eta_1/\eta_2 = 0.916$ [*Handa*, 1990; *Ripmeester and Ratcliffe*, 1988].

A3. Sensitivity of Computed Solubility to Volumetric Parameters

Regardless of the thermodynamic model used, the solubility computed within the hydrate stability field is, in fact, an extrapolation from experimental values acquired in the same temperature range but outside of the hydrate stability field. The precision of the extrapolation is thus limited by the accuracy of water and gas partial volumes in the liquid phase and of the volume of the unit cell in the hydrate lattice.

The relationship between methane fugacity and solubility given by *Duan et al.* [1992] can be rewritten as

$$\ln f = \ln m_{CH_4} + \mu^l_{CH_4}(T,P_0)/RT + \int_{P_0}^{P} V^l_{CH_4}(T,P)dP \quad \text{(A5)}$$

where $\mu^l_{CH_4}(T,P_0)$ is the chemical potential of CH_4 in solution at a reference pressure and $V^l_{CH_4}$ is the partial volume of methane in solution. The computed partial volume of methane in solution compares well with data at elevated pressure and temperature [*Duan et al.*, 1992] but, at 0°C, is slightly smaller than those reported by *Handa* [1990] (32 $cm^3\ mol^{-1}$ versus 34.5 $cm^3\ mol^{-1}$). The pressure term in (5) represents the effect of pressure on the stability of the empty hydrate lattice:

$$(\mu_\beta - \mu_L)(P,T) = (\mu_\beta - \mu_L)(0,T) + \int_0^P \frac{(V_\beta - V_L)}{RT} dP \quad \text{(A6)}$$

If $(V_\beta - V_L)$ is computed as given by *Handa* [1990], the most significant variation in the 0-50 MPa 0°-25°C domain is due to the compressibility of liquid water: $(V_\beta - V_L)$ varies from 4.5

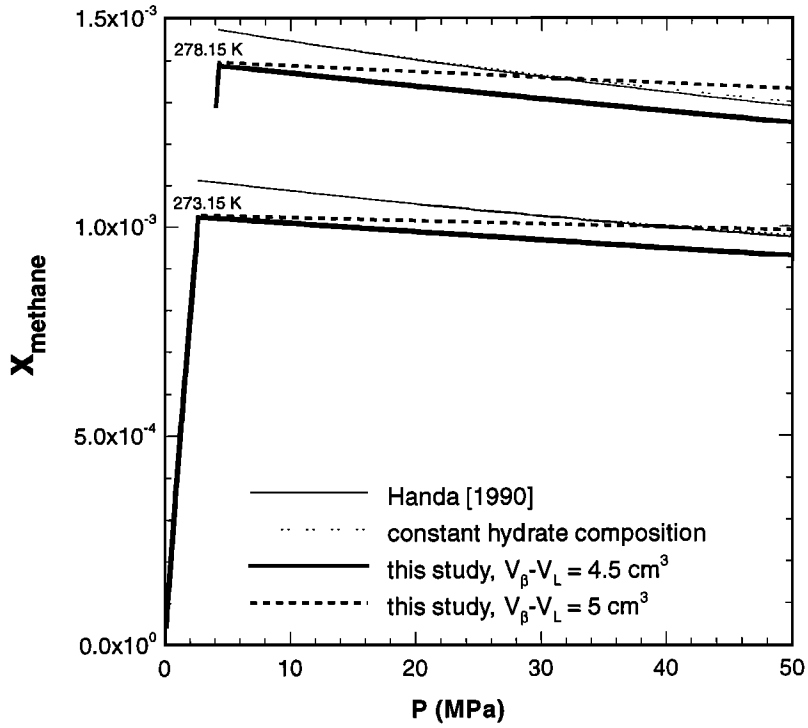

Figure A2. Methane solubility in the hydrate stability field as a function of pressure computed by *Handa* [1990] is compared with results of models with more drastic approximations: constant hydrate composition with six water molecules per methane molecule and (this model) constant molar volume difference between liquid water and hydrate lattice (but taking variations of hydrate composition with pressure and temperature into account).

cm^3/mol at low pressures to 5 cm^3/mol at 50 MPa. Variation as a function of temperature is much smaller. Figure A2 compares the curves of *Handa* [1990] (and an approximation using (1) in main text and $n = 6$) with the output of the model presented above, assuming constant molar volumes. The solubility curves are offset because the values given by the methane solubility model [*Duan, et al.*, 1992] are slightly lower than the experimentally derived values of *Handa* [1990]. The slope dx_s/dp appears quite sensitive to $(V_\beta - V_L)$. One limitation of our model is that changing the volumetric parameters would require adjustment of the other parameters to keep the correct prediction of the three-phase equilibrium. For this reason, the original and constant value of 4.6 cm^3/mol was used. Although the computational results are less precise at 0°C than Handa's, they are acceptable for our purpose.

A4. Correction for Water Salinity

Dissolved salts decrease the temperature of hydrate dissociation (at a given pressure) because they decrease the activity of water in solution. The presence of dissolved salts also decreases the solubility of methane for a given gas phase fugacity but because the chemical potential of water in the hydrate phase is a function of methane fugacity, (equation (A3)), this decrease of methane solubility has no effect on the three-phases equilibrium curve. The water activity term appears in (A4) and can be computed from models of electrolyte mixtures [*Patwardan and Kumar*, 1986; *Pitzer*, 1991]. Several published models of hydrate stability include such complete computations [*Dickens and Quinby-Hunt*, 1997; *Englezos and Bishnoi*, 1988; *Tohidi et al.*, 1995], but a simple approach is used here: water phase activity for standard seawater at various concentrations are interpolated from a table from *Weast* [1980]. For a salinity of 30‰ the correction (-ln a_w) is 0.0158, compared with 0.0161 of *Dickens and Quinby-Hunt* [1997], and the temperature shift of the hydrate dissociation curve is the same as obtained by them (Figure A1). Pore fluid composition may be significantly different from that of seawater due to sulfate reduction, carbonate precipitation, and other interactions with the solids, but *Dickens and Quinby-Hunt* [1997] found that the effects of the simultaneous removal of sulphate and of divalent cations (Mg^{2+}, Ca^{2+}) typically observed in euxinic pore fluids nearly compensate each other.

Notation

P pressure (liquid phase pore pressure).
T temperature.
n number of water molecules per methane molecule in the hydrate.
ν_i number of cavities of type i per molecule of water.
η_1, η_2 hydrate cage occupancies.
f methane fugacity.
C_i Langmuir constants.
H enthalpy.
μ_L chemical potential of water in pore fluid.
μ_β chemical potential of empty hydrate lattice.
μ_H chemical potential of water in methane-bearing hydrate.
x_{CH_4} methane solubility in mole fraction.
m_{CH_4} methane solubility mol kg-1.
V_β molar volume of water in the hydrate lattice.
V_L partial molar volume of water in the liquid phase.

$V^l_{CH_4}$ partial molar volume of methane in the liquid phase.
ΔV volume change when hydrate is formed out of dissolved methane.
a_w water activity in bulk liquid phase.
P_g gas pressure.
r pore radius.
θ wetting angle.
γ_{ab} interfacial energy between phases *a* and *b*.
S surface area of interface.
G free energy.
P_{hydr} hydrostatic pressure.
P_{lith} lithostatic pressure.
P_c capillary pressure.
P_i internal pressure in hydrate phase.
σ_3, σ_1 minimum and maximum principal stresses.
K_0 stress ratio for uniaxial consolidation.
φ porosity.
z depth.
S_h fraction of pore space filled with hydrate phase.
S_g fraction of pore space filled with gas phase.

Acknowledgments. We thank Bill Winters at USGS (Woods Hole) for kindly providing us with samples from Blake Ridge, Diane Condliffe and Richard Jones at Rock Deformation Research, Leeds University, who performed the mercury injection tests, G. D. Ginsburg (Research Institute for Geology and Mineral Resources of the Ocean, St Petersburg) for useful discussions and for giving us access to preliminary grain size data from Blake Ridge ODP holes, A. Rempel for his comments on an earlier version of the manuscript, and G. Dickens, M. Kohn, and O. Zatsepina for their constructive reviews.

References

Andreassen, K., P.E. Hart, and A. Grantz, Seismic studies of a bottom simulating reflection related to gas hydrate beneath the continental margin of the Beaufort Sea, *J. Geophys. Res., 100*, 12659-12673, 1995.

Arnould, M., M. Audiguier, P. Delage, F.-M. Pellerin, R. Struillou, and B. Vayssade, Study of clayey soils by mercury porosimetry: Testing of structural variations under varying conditions, *Bull. Asssoc Int. Géol. Ing., 22*, 213-223, 1980.

Bray, C.J., and D.E. Karig, Porosity of sediments in accretionary prisms and some implications for dewatering processes, *J. Geophys. Res., 90*, 768-778, 1985.

Bishnoi, P.R., A.K. Gupta, P. Englezos, and N. Kalogerakis, Multiphase equilibrium flash calculations for systems containing hydrates, *Fluid Phase Equilibria, 53*, 97-104, 1989.

Clennell, M.B., M. Hovland, D. Lysne, and J.S. Booth, Role of capillary forces, coupled flows and sediment-water depletion in the habitat of gas hydrate (abstract), *Eos Trans. AGU, 76*(17), Spring Meet. Suppl., S164-S165, 1995.

Clennell, M.B., M. Hovland, J.S. Booth, P. Henry, and W.J. Winters, Formation of natural gas hydrates in marine sediments, 1, Conceptual model of gas hydrate growth conditionned by host sediment properties, *J. Geophys. Res.*, this issue.

Defay, R., I. Prigogine, A Bellemans, and D.H. Everett, *Surface Tension and Adsorption*, Longmans, Green, Toronto, 1966.

Dickens, G.R. and M.S. Quinby-Hunt, Methane hydrate stability in pore water: A simple theoretical approach for geophysical applications, *J. Geophys. Res., 102*, 773-783, 1997.

Dickens, G.R., M.M. Castillo, and J.C.G. Walker, A blast of gas in the latest Paleocene: Simulating first order effects of massive dissociation of oceanic methane hydrate, *Geology, 25*, 623-626, 1997a.

Dickens, G. R., C.K. Paull, P. Wallace, and Leg 164 Scientific Party, Direct measurement of in situ methane quantities in a large gas hydrate reservoir, *Nature, 385*, 426-428, 1997b.

Duan, Z., N. Møller, J. Greenberg, and J.H. Weare, The prediction of methane solubility in natural waters to high ionic strength from 0° to 250°C and from 0 to 1600 bar, *Geochim. Cosmochim. Acta, 56*, 1451-1460, 1992.

Emschwiller, G., *Chimie Physique*, vol. 2, *Equilibre en Solutions - Phénomènes de surface*, pp. 791-796, Presses Univ. de Fr., Paris, 1961.

Englezos, P., and P.R. Bishnoi, Prediction of gas hydrate formation conditions in aqueous electrolyte solutions, *AIChE J., 34*, 1718-1721, 1988.

Everett, D.H., The themodynamics of frost damage to porous solids, *Trans. Faraday Soc., 57*, 1541-1551, 1961.

Ginsburg, G.D., and V.A. Soloviev, Methane migration within the submarine gas-hydrate stability zone under deep-water conditions, *Mar. Geol., 137*, 49-57, 1997.

Ginsburg, G.D., and V.A. Soloviev, *Submarine Gas Hydrates*, 216 pp., 1998, VNIIOkeangeologia / Norma, St. Petersburg.

Ginsburg, G.D., V.A. Soloviev, T. Matveeva, and I. Andreeva, Sediment grain-size control on gas hydrate presence, ODP Sites 994, 995, and 997, *Proc. Ocean Drill. Program, Sci. Results, 164*, in press, 1999.

Griffiths, F.J., and R.C. Joshi, Change in pore size due to secondary consolidation of clays. *Can. Geotech. J., 28*, 20-24, 1991.

Handa, Y.P., Effect of hydrostatic pressure and salinity on the stability of gas hydrates, *J. Phys. Chem., 94*, 2653-2657, 1990.

Handa, Y.P., and D. Stupin, Thermodynamic properties and dissociation characteristics of methane and propane hydrates in 70-Å-radius silica gel pores, *J. Phys. Chem., 96*, 8599-8603, 1992.

Handa, Y.P., M. Zakrzewski, and C. Fairbridge, Effect of restricted geometries on the structure and thermodynamic properties of ice, *J. Phys. Chem., 96*, 8594-8599, 1992.

Henry, P., Relationship between porosity, electrical conductivity, and cation exchange capacity in Barbados wedge sediments, *Proc. Ocean Drill. Program, Sci. Results, 156*, 137-149, 1998.

Holbrook, W.S., H. Hoskins, W.T. Wood, R.A. Stephen, D. Lizarralde, and Leg 164 Scientific Party, Methane hydrate and free gas on the blake ridge from vertical seismic profiling, *Science, 273*, 1840-1843, 1996.

Holder, G.D., S.P. Zetts, and N. Pradhan, Phase behaviour in systems containing clathrate hydrates, *Rev. Chem. Eng., 5*, 1-70, 1988.

Hovland, M., D. Lysne, and M.J. Whiticar, Gas hydrate and sediment gas composition, Hole 892A, *Proc.Ocean Drill. Program, Sci. Res., 146*, 151-161, 1995.

Hyndman, R.D., and E.E. Davis, A mechanism for the formation of methane hydrate and seafloor bottom-simulating reflectors by vertical fluid expulsion, *J. Geophys. Res., 97*, 7025-7041, 1992.

Hyndman, R.D., J.P. Foucher, M. Yamano, A. Fisher, and Scientific Team of Ocean Drilling Program Leg 131, Deep sea bottom-simulating reflectors: Calibration of the base of the hydrate stability field as used for heat flow estimates, *Earth Planet. Sci. Lett., 109*, 289-301, 1992.

Jones, M.E., Mechanical principles of sediment deformation, in *The Geological Deformation of Sediments*, edited by A.J. Maltman, pp. 37-71, Prentice-Hall, Englewood Cliffs, N.J., 1994.

Karig, D.E., and G. Hou, High-stress consolidation experiments and their geologic implications, *J. Geophys. Res., 97*, 289-300, 1992.

Kastner, M., K.A. Kvenvolden, M.J. Whiticar, A. Camerlinghi, and T.D. Lorenson, Organic geochemistry of gases, fluids and hydrates at the Cascadia accretionary margin, *Proc. Ocean Drill. Program, Sci. Res., 146*, 175-189, 1995.

Katz, A.J., and A.H. Thompson, Predition of rock electrical condutivity from mercury injection measurements, *J. Geophys. Res., 92*, 599-607, 1987.

Katzman, R., W.S. Holbrook, and C.K. Paull, Combined vertical-incidence and wide-angle seismic study of a gas-hydrate zone, *J. Geophys. Res., 99*, 17975-17995, 1994.

Kraemer, L.M., R.M. Owen, and G.R. Dickens, Litholoy of the upper gas hydrate zone at Site 994C, Blake Outer Ridge, *Proc. Ocean Drill. Program, Sci. Results, 164*, in press, 1999.

Kvenvolden, K.A., Methane hydrate: A major reservoir of carbon in the shallow geosphere, *Chem. Geol., 71*, 41-51, 1988.

Le Pichon, X., P. Henry, and S. Lallemant, Water flow in the Barbados Accretionary Complex, *J. Geophys. Res., 95*, 8945-8967, 1990.

Lee, M.W., D.R. Hutchinson, W.P. Dillon, J.J. Miller, W.F. Agena, and B.A. Swift, Method of estimating the amount of in situ gas hydrates in deep marine sediments, *Mar. Pet. Geol., 10*, 493-506, 1993.

Lowell, S. and J. E. Shields, *Powder Surface Area and Porosity*, pp. 121-135, Chapman and Hall, New York, 1984.

MacKay, M.E., R.D. Jarrard, G.K. Westbrook, R.D. Hyndman, and Shipboard Party of ODP Leg 146, Origin of bottom-simulating

reflectors: Geophysical evidence from the Cascadia accretionary prism, *Geology*, *22*, 459-462, 1994.

Miller, S.L., The nature and occurrence of clathrate hydrates, in *Natural Gases in Marine Sediments*, edited by I.R. Kaplan, pp. 151-177, Plenum, New York, 1974.

Miller, S.L., Clathrate hydrates in the solar system, in *Ices in the Solar System*, edited by J. Klinger et al., pp. 59-79, D. Reidel, Norwell, Mass., 1985.

Minshull, T.A., S.C. Singh, and G.K. Westbrook, Seismic velocity structure at a gas hydrate reflector, offshore western Columbia, from full waveform inversion, *J. Geophys. Res.*, *99*, 4715-4734, 1994.

Munck, J., S. Skold-Jørgensen, and P. Rasmussen, Computations of the formation of gas hydrates, *Chem. Eng.*, *43*, 2661-2672, 1988.

Patwardan, V.S., and A. Kumar, A united approach for prediction of thermodynamic properties of aqueous mixed-electrolyte solutions, I, Vapor pressure and heat of vaporisation, *AIChE J.*, *32*, 432-434, 1986.

Paull, C. K., W. Ussler III and W. P. Dillon, Is the extend of glaciation limited by marine gas-hydrate?, *Geophys. Res. Lett.*, *18*, 432-434, 1991.

Paull, C.K., et al., *Proceedings of Ocean Drilling Program, Initial Reports*, vol. 164, Ocean Drill. Program, College Station, Tex., 1996.

Pellerin, F.-M., La porosimetrie au mercure appliquée à l'étude géotechnique des sols et des roches, *Bull. Liaison Lab. Ponts et Chaussées*, *106*, 105-116, 1980.

Pitzer, K.S. (Ed.), Ion interaction approach: Theory and data correlaton, in *Activity Coefficients in Electrolyte Solutions*, pp. 75-153, CRC Press, Boca Raton, Fla., 1991.

Portsmouth, R.L., and L.F. Gladden, Determination of pore connectivity by mercury porosimetry, *Chem. Eng. Sci.*, *46*, 3023-3026, 1991.

Rempel, A., and B.A. Buffett, Formation and accumulation of gas hydrate in porous media, *J. Geophys. Res.*, *102*, 10151-10164, 1997.

Revil, A., and P.W.J. Glover, Theory of ionic surface electrical conduction in porous media, *Phys. Rev. B*, *55*, 1757-1772, 1997.

Ripmeester, J.A. and C.L. Ratcliffe, *J. Phys. Chem.*, *92*, 337-343, 1988.

Rowe, M.M. and J.F. Gettrust, Faulted structure of the bottom simulating reflecor on Blake Ridge, western North Atlantic, *Geology*, *21*, 833-836, 1993.

Ruppel, C., Anomalously cold temperature observed at the base of the gas hydrate stability zone on the U.S. Atlantic passive margin, *Geology*, *25*, 699-702, 1997.

Singh, S.C., and T.A. Minshull, Velocity structure of a gas hydrate reflector at Ocean Drilling Program Site 889 from a lobal seismic waveform inversion, *J. Geophys. Res.*, *99*, 24221-24233, 1994.

Singh, S.C., T.A. Minshull, and G.D. Spence, Velocity structure of a gas hydrate reflector, *Science*, *260*, 204-207, 1993.

Sloan, E.D., *Clathrate Hydrates of Natural Gases*, Marcel Dekker, New York, 1990.

Tissot, B.O., and D.H. Welte, *Petroleum Formation and Occurence*, 538 pp., Springer-Verlag, New York, 1978.

Tohidi, B., A. Danesh, and A.C. Todd, Modelling single and mixed electrolyte solutions and its applications to gas hydrates, *Trans. Inst. Chem. Eng.*, *73*, 464-465, 1995.

Van der Waals, J. H., and J.C. Platteeuw, Clathrate solutions, *Adv. Chem. Phys.*, 2, 1-57, 1959.

Washburn, E.W., The dynamics of capillary flow, *Phys. Rev.*, *17*, 273-283, 1921.

Weast, R.C., *CRC Hanbook of Chemistry and Physics*, 61st edition, pp. D-258, CRC Press, Boca Raton, 1980.

Whiticar, M.J., M. Hovland, M. Kastner, and J.C. Sample, Organic geochemistry of gases, fluids and hydrates at the Cascadia accretionary margin, *Proc. Ocean Drill. Program, Sci. Results*, *146*, 385-397, 1995.

Xu, W., and C. Ruppel, Predicting the occurrence, distribution, and evolution of methane gas hydrate in porous marine sediments, *J. Geophys. Res.*, 104, 5081-5095, 1999.

Yousif, M.H., and E.D. Sloan, Experimental investigation of hydrate formation and dissociation in consolidated porous media, *SPE Reservoir Eng.*, *6*, 452-458, 1991.

Yuan, T., R.D. Hyndman, G.D Spence, and B. Desmons, Seismic velocity increase and deep-sea hydrate concentration above a bottom-simulating reflector on the northern Cascadia continental slope, *J. Geophys. Res.*, *101*, 13655-13671, 1996.

Zatsepina, O.Y., and B.A. Buffett, Phase equilibrium of gas hydrate: Implication for the formation of hydrate in the deep sea floor, *Geophys. Res. Lett.*, *24*, 1567-1570, 1997.

Zatsepina, O.Y., and B.A. Buffett, Thermodynamic conditions for the stability of gas hydrate in the seafloor, *J. Geophys. Res.*, *103*, 24127-24139, 1998.

M. B. Clennell, Centro de Pesquisa em Geofisica e Geologia, Universidade Federal da Bahia, 123 Rua Caetano Moura, Salvador, Bahia 40210-340, Brasil. (clennell@cpgg.ufba.br)

P. Henry, Laboratoire de Géologie, Ecole Normale Supérieure, 24 rue Lhomond, 75231 Paris Cedex 05, France. (henry@geologie.ens.fr)

M. Thomas, Physico-chimie appliquée, Institut Français du Pétrole, 1-4 Av de Bois Préau, 92852 Rueil-Malmaison Cedex, France. (Michel.THOMAS@ifp.fr)

(Received May 22, 1998; revised April 27, 1999;
accepted May 5, 1999)